Radiometric Tracking Techniques for Deep-Space Navigation

Catherine L. Thornton
James S. Border

MONOGRAPH 1
DEEP–SPACE COMMUNICATIONS AND NAVIGATION SERIES

Radiometric Tracking Techniques for Deep-Space Navigation

DEEP-SPACE COMMUNICATIONS AND NAVIGATION SERIES

Issued by the Deep-Space Communications and Navigation Systems
Center of Excellence
Jet Propulsion Laboratory
California Institute of Technology

Joseph H. Yuen, Editor-in-Chief

Radiometric Tracking Techniques for Deep-Space Navigation

Catherine L. Thornton
James S. Border

Jet Propulsion Laboratory
California Institute of Technology

MONOGRAPH 1
DEEP–SPACE COMMUNICATIONS AND NAVIGATION SERIES

Radiometric Tracking Techniques for Deep-Space Navigation
(JPL Publication 00-11)

October 2000

The research described in this publication was carried out at the
Jet Propulsion Laboratory, California Institute of Technology,
under a contract with the National Aeronautics and Space Administration.

Table of Contents

Foreword

The Deep Space Communications and Navigation Systems Center of Excellence (DESCANSO) was recently established for the National Aeronautics and Space Administration (NASA) at the California Institute of Technology's Jet Propulsion Laboratory (JPL). DESCANSO is chartered to harness and promote excellence and innovation to meet the communications and navigation needs of future deep-space exploration.

DESCANSO's vision is to achieve continuous communications and precise navigation—any time, anywhere. In support of that vision, DESCANSO aims to seek out and advocate new concepts, systems, and technologies; foster key scientific and technical talents; and sponsor seminars, workshops, and symposia to facilitate interaction and idea exchange.

The Deep Space Communications and Navigation Series, authored by scientists and engineers with many years of experience in their respective fields, lays a foundation for innovation by communicating state-of-the-art knowledge in key technologies. The series also captures fundamental principles and practices developed during decades of deep-space exploration at JPL. In addition, it celebrates successes and imparts lessons learned. Finally, the series will serve to guide a new generation of scientists and engineers.

Joseph H. Yuen
DESCANSO Leader
October 2000

Preface

Radiometric Tracking Techniques for Deep Space Navigation is an introduction to newcomers in this field, a reference to professionals in related fields, and an exposition of the current state of the art. It focuses on a broad array of technologies and concepts developed over the last four decades to support radio navigation of interplanetary spacecraft. The technical terms in the text assume that the reader is familiar with basic engineering and mathematical concepts contained in books such as *The Electronics of Radio* (D. B. Rutledge, Cambridge University Press, 1999) and *Applied Optimal Estimation* (A. Gelb, editor, MIT Press, 1974).

In addition to an overview of Earth-based radio navigation techniques, the scope of this monograph includes a simplified conceptual presentation of each radiometric measurement type, its information content, and expected measurement accuracy. More rigorous treatments may be found in the numerous references cited. Many of these references pertain to work done at the Jet Propulsion Laboratory (JPL) as part of the development of the very system that is the topic of this monograph.

Beyond describing the types of radio measurements that *could* be made, we also suggest what measurements *should* be made under various mission conditions. The methods we describe for both acquiring and calibrating radiometric measurements provide a robust system to support guidance and navigation for future robotic space exploration.

We have drawn the content of this monograph from the work of many JPL colleagues, past and present, in the Tracking Systems and Application Section and the Navigation and Flight Mechanics Section, who have participated in the effort to develop and use state-of-the-art radiometric navigation techniques. We are especially indebted to William G. Melbourne for

his analyses, leadership, and publications during the early, formative years of this technical discipline. We are also indebted to many others who have played a crucial role in system engineering, hardware fabrication, and system operations. Finally, we acknowledge the primary role of NASA, its Deep Space Network, and numerous planetary flight projects, in the development of this exciting technical field.

Catherine L. Thornton
James S. Border
October 2000

Acknowledgments

We would like to express our appreciation to Joseph H. Yuen for his encouragement and support during the writing of this monograph. We are also indebted to Diana M. Meyers for her thorough reading and editing of the manuscript and to Mary E. Young for expert desktop publishing. We are especially grateful to the following individuals for technical information, advice, and helpful suggestions during the preparation of the manuscript: Yoaz E. Bar-Sever, Laureano A. Cangahuala, Jean O. Dickey, William M. Folkner, Richard S. Gross, Christopher S. Jacobs, David C. Jefferson, Robert D. Kahn, Stephen M. Lichten, Ulf Lindqwister, Anthony J. Mannucci, Timothy P. McElrath, Theodore D. Moyer, George M. Resch, Thomas F. Runge, J. Alan Steppe, Robert L. Tjoelker, Yvonne Vigue-Rodi, Bobby G. Williams, Brian D. Wilson, Lincoln J. Wood, Sien-Chong Wu, Lawrence E. Young, and James F. Zumberge.

Chapter 1
Introduction

Tracking of vehicles in deep space, that is, at lunar or planetary distances, is accomplished through a variety of radio and optical techniques. Since the 1970s, the particular mix of data types used for interplanetary navigation has depended largely upon where the spacecraft was located along its flight path. For example, during the cruise phase of a mission, roughly from the time of injection into the interplanetary transfer orbit until approach to the target body, Earth-based radiometric tracking techniques are typically used. Radio tracking systems are called upon to provide highly accurate orbit information to support midcourse trajectory corrections and early probe releases. During the approach phase, these Earth-based observables may be used in conjunction with onboard optical images of the target or one of its satellites against a known star background. The optical images provide a direct measure of spacecraft position relative to the target and are an important complement to Earth-based radio tracking, especially when there is a large uncertainty in the target-body ephemeris.

There are some notable exceptions to this standard model for navigation tracking. In fact, a number of recent missions designed with tight cost constraints have relied solely upon radio tracking, even during the encounter phase, for example, Mars Pathfinder, Mars Climate Orbiter, and Mars Polar Lander. And the New Millenium mission Deep Space 1 (DS-1) successfully demonstrated autonomous, onboard cruise navigation, using optical-only measurements [1,2].

Future missions will use a mix of tracking data types appropriate to meet specific project requirements. These missions will benefit from the availability of a variety of precise, reliable tracking techniques to enable more challenging navigation performance or to provide complementary information in unexpected, difficult spaceflight situations.

This monograph focuses primarily upon the fundamentals of Earth-based radiometric tracking as applied to deep space navigation. Basic concepts of orbit determination are introduced in Chapter 2. A standard reference frame is defined; parameters that constrain a spacecraft trajectory are identified; and standard models associated with Earth-based tracking are discussed.

Until the 1980s, deep space radio tracking relied solely upon Doppler and range systems. The improvement in performance of these systems is reviewed in Chapter 3. The information content of each measurement is also discussed, and limiting error sources are identified.

Inherent limitations to conventional Doppler and range tracking prompted the development in the 1970s of a technique known as very long baseline interferometry (VLBI). This technique, already well known to radio astronomers, was first applied to spacecraft tracking during the late 1970s and was subsequently used by the Voyager project to support the Uranus and Neptune encounters. The VLBI system developed for navigating missions such as Galileo and Mars Observer in the 1990s provided a direct geometric measure of spacecraft angular position—in some situations, at least five times more accurate than that determined from several days of Doppler and range data. VLBI tracking concepts are introduced in Chapter 4. The advantages of this data type for angular positioning are described, and major error sources are identified.

Missions beyond the year 2000 will have ever-increasing requirements for improved radiometric tracking performance. These missions will be faced with issues related to navigation system robustness, reliability, and timeliness, as well as accuracy and cost effectiveness. Expected needs for rapid, onboard responses will place new demands on both optical and radio tracking technologies. Chapter 5 examines expected radio tracking system improvements motivated by expected future challenges, such as tight targeting requirements at Mars to enable aerocapture and precise descent and landing, navigating low-thrust missions with imperfectly modeled spacecraft forces, and precisely landing a sample return mission on Earth.

References

[1] S. Bhaskaran et al., "In-flight Performance Evaluation of the Deep Space 1 Autonomous Navigation System," MS00/53, *Proceedings of the International Symposium on Spaceflight Dynamics,* Biarritz, France, June 26–30, 2000.

[2] J. E. Riedel et al., "Using Autonomous Navigation for Interplanetary Missions: The Validation of Deep Space 1 Autonav," IAA-L-0807, *Fourth International Conference on Low-Cost Planetary Missions,* Laurel, Maryland, May 2–5, 2000.

Chapter 2
Earth-Based Tracking and Navigation Overview

2.1 Navigation Process

The process of spacecraft navigation is illustrated in Fig. 2-1. The two primary navigation functions are orbit determination and guidance. The orbit determination process is an iterative procedure requiring an a priori estimate of the spacecraft trajectory, referred to as the nominal orbit. Expected values of the tracking observables are calculated, based upon nominal values for the trajectory and precise models of the tracking observables. These calculated observables are differenced with the actual values obtained from the tracking system to form the data residuals.

If the trajectory and the data models were perfectly known, the residuals would exhibit a purely random, essentially Gaussian, distribution due to uncorrelated measurement errors (for example, thermal noise in the tracking receiver). However, errors in the trajectory and the observable models introduce distinctive signatures in the residuals. These signatures enable an adjustment to the model parameters through a procedure known as weighted linear least-squares estimation, in which the optimal solution is defined to be the set of parameter values that minimizes the weighted sum of squares of residuals. When the data are weighted by the inverse of their error covariance, the procedure yields a minimum variance estimator [1]. Since this procedure represents a linear solution to a nonlinear problem, the steps must be iterated, using the latest parameter estimates, until the solution converges.

The accuracy of the solutions obtained in the manner explained above may be assessed through a variety of tests. The calculated, or formal, uncertainties

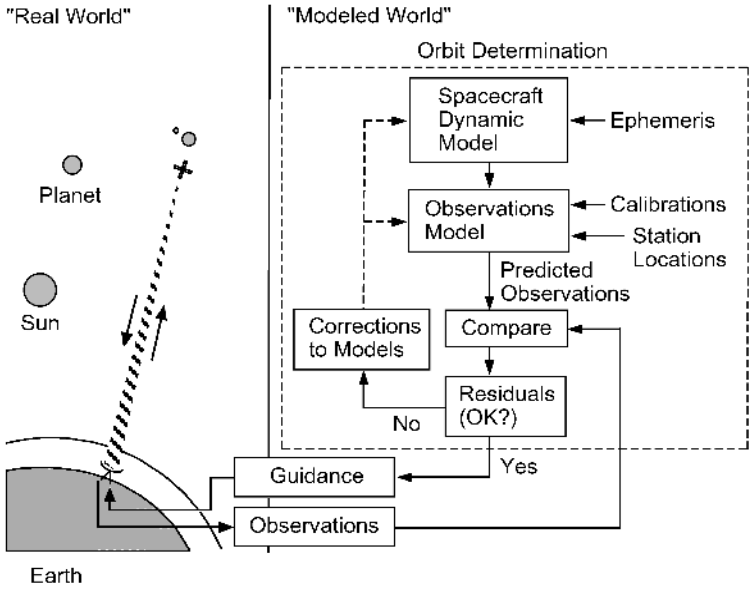

Fig. 2-1. The navigation process. Orbit determination is an iterative procedure for estimating the spacecraft trajectory and related physical parameters from a set of tracking data. Guidance involves the calculation of optimal maneuvers and commands needed to deliver the spacecraft to the desired target.

are obtained from the least-squares algorithm in the form of a parameter-error covariance matrix [1]. The postfit residuals (that is, the residuals calculated from the weighted least-squares solution) are examined for systematic trends and/or large scatter relative to the expected data noise. A more concrete test involves the subsequent acquisition of additional tracking data and an assessment of the behavior of the predicted, or unadjusted, residuals. Other tests involve comparing solutions obtained from different mixes of tracking data, model parameters, and so forth. Large variations in such solutions, relative to the calculated formal uncertainties, are strong indications of model errors, either in the tracking data or in the spacecraft dynamics.

Once the navigators are confident that the trajectory can be reliably predicted, guidance algorithms are executed to calculate any necessary retargeting maneuvers, and reoptimization of the trajectory may be performed, as necessary. The orbit-determination and guidance functions are repeated, as required, during interplanetary flight until the spacecraft is accurately delivered to the target body. Delivery accuracy requirements vary from mission to mission, but typically become increasingly more challenging as demonstrated navigation performance improves. For example, the one sigma (standard deviation) delivery requirement for the Voyager Io encounter was approximately

900 km [2]. The comparable value for the first Galileo Io encounter was about 100 km [3].

2.2 Reference Frames

As astronomical measurement accuracies have improved, understanding and definitions of reference frames have evolved from simple geometric concepts to abstract, implicitly defined constructs. What follows is an introduction to reference frames, using historical concepts. A more rigorous approach is described at the end of this section.

Discussion of Earth-based tracking capabilities is most readily accomplished using a geocentric equatorial reference system such as the one shown in Fig. 2-2. In this system, Earth is located at the center of a celestial sphere. Earth's equator is the plane of reference, and the celestial poles are defined by an extension of Earth's axis of rotation.

The plane that contains the celestial poles and an object, for example, a spacecraft, describes a great circle on the celestial sphere. The point at which

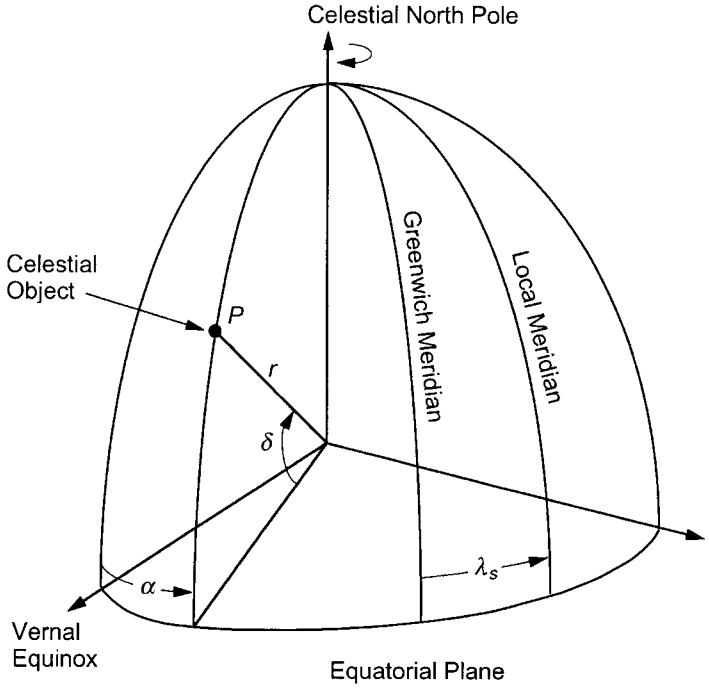

Fig. 2-2. Geocentric equatorial reference frame. The spherical coordinates of an object, *P*, are given by the geocentric range, *r*, and the angles α (right ascension) and δ (declination).

this circle intersects the celestial equator defines the right ascension of the object, α, measured easterly from the vernal equinox. The angular distance of the object from the equator measured on the great circle is termed the declination, δ. The declination varies from –90 deg to +90 deg with a positive angle indicating that the object is north of the equator.

The reference point for measurement of right ascension is defined by the intersection of Earth's equator and the ecliptic, the plane in which Earth moves about the Sun. The point where the Sun crosses the equator on its apparent path northward is termed the vernal equinox. This point, however, gradually moves with time, due to precession of Earth's axis about the pole of the ecliptic. Therefore, the vernal equinox must be defined as of a specific date. The current internationally accepted epoch is 12:00 on January 1 of the year 2000, or Julian date 2451545.0, and is referred to as J2000. This epoch has been adopted by the International Astronomical Union (IAU) and the International Earth Rotation Service (IERS) along with a set of standards for precession and nutation of Earth's pole and other physical models and constants associated with Earth-based observation systems [4–8].

Measurements from stations fixed on Earth are best described in an Earth-fixed (terrestial) reference frame (see Section 3.3.4). In this terrestial frame, points on Earth are located relative to the instantaneous Earth pole and equator, and a great circle that passes through Greenwich, known as the prime meridian (see Fig. 2-2). Spacecraft positions, on the other hand, are calculated in a space-fixed (celestial) reference frame associated with the planetary ephemeris. This celestial reference frame is typically a solar system barycentric frame aligned with the mean Earth equator and equinox of J2000 [9]. Transformations between the terrestial and celestial frames are carefully modeled and accounted for in the orbit-determination process [9]. Tracking-system calibrations that support these transformations are described in Sections 3.3.4 and 4.1.

Today, the celestial reference frame is defined by the positions of quasars in the International Celestial Reference Frame (ICRF) [10]. The origin of right ascension is a certain linear combination of catalog coordinates. The equator and the equinox are now measured quantities. Planetary ephemerides are constrained to be consistent with this definition to within current knowledge. For a more in-depth discussion of reference frames, see references 10–15 and the references therein.

2.3 Spacecraft Equations of Motion

Spacecraft trajectories are calculated by integrating the equations of motion in the celestial reference frame adopted by the project. This frame is implicitly defined by the current planetary ephemeris and is closely aligned with the ICRF [15,16].

In the trajectory computations, all known dynamical influences on the spacecraft are accounted for. These include all solar system gravitational accelerations and all nongravitational forces such as solar radiation pressure, attitude control thrusts, and gas leaks from the spacecraft control jets. Accurate representation of these forces can require detailed modeling of spacecraft features such as reflective surfaces, heat radiation characteristics, and thruster units. Initial conditions for the equations of motion are the six parameters representing spacecraft position and velocity at a specific epoch. This initial state may be expressed in a variety of forms within the adopted reference frame, for example, using Cartesian or spherical coordinates, or in terms of classical Keplerian elements. It is convenient in the ensuing discussion of Earth-based tracking to refer to the spherical coordinates (r, α, δ, $\dot{r}$, $\dot{\alpha}$, $\dot{\delta}$) in the geocentric Earth equatorial system of Fig. 2-2.

Given perfect knowledge of all forces and purely random measurement errors, a navigator must estimate only six parameters (r, α, δ, $\dot{r}$, $\dot{\alpha}$, $\dot{\delta}$) to determine a spacecraft orbit. The real world is not so kind, however. A more typical scenario requires simultaneous determination of spacecraft state and selected parameters of the force models. It is also usually necessary to estimate a number of model parameters associated with calculation of the tracking observables. These models are the focus of the next chapter.

References

[1] G. J. Bierman, *Factorization Methods for Discrete Sequential Estimation,* Mathematics in Science and Engineering, vol. 128, New York: Academic Press, 1977.

[2] J. P. McDanell et al., *Voyager Orbit Determination Strategy and Accuracy,* Voyager Project Document 618-118 (internal document), Jet Propulsion Laboratory, Pasadena, California, 1977.

[3] *Galileo Navigation Plan,* Galileo Project Document 625-566, Rev. A, JPL D-649, Rev. A (internal document), Jet Propulsion Laboratory, Pasadena, California, October 1989.

[4] D. D. McCarthy, editor, *IERS Standards (1992): IERS Technical Note 3,* Paris: Observatoire de Paris, 1992.

[5] D. D. McCarthy, editor, *IERS Standards (1996): IERS Technical Note 21,* Paris: Observatoire de Paris, 1996.

[6] P. K. Seidelmann, "1980 IAU Theory of Nutation: The Final Report of the IAU Working Group on Nutation," *Celestial Mechanics,* vol. 27, no. 1, pp. 79–106, May 1982.

[7] J. H. Lieske et al., "Expressions for the Precession Quantities Based upon the IAU (1976) System of Astronomical Constants," *Astronomy and Astrophysics,* vol. 58, no. 1–2, pp.1–16, June 1977.

[8] J. H. Lieske, "Precession Matrix Based upon IAU (1976) System of Astronomical Constants," *Astronomy and Astrophysics,* vol. 73, no. 3, pp. 282–284, March 1979.

[9] T. D. Moyer, *Formulation for Observed and Computed Values of Deep Space Network Data Types,* JPL Publication 00-7, Jet Propulsion Laboratory, Pasadena, California, October 2000.

[10] C. Ma et al., "The International Celestial Reference Frame as Realized by Very Long Baseline Interferometry," *The Astronomical Journal,* vol. 116, no. 1, pp. 516–546, July 1998.

[11] O. J. Sovers and C. S. Jacobs, *Observation Model and Parameter Partials for the JPL VLBI Parameter Estimation Software MODEST—1996,* JPL Publication 83-39, Rev. 6, Jet Propulsion Laboratory, Pasadena, California, August 1996.

[12] *1998 IERS Annual Report,* Paris: Observatoire de Paris, 1999.

[13] E. M. Standish, "Celestial Reference Frames: Definitions and Accuracies," chapter in *The Impact of VLBI on Astrophysics and Geophysics* (M. J. Reid and J. M. Moran, editors), proceedings of the 129th IAU Symposium, Cambridge, Massachusetts, May 10–15, 1987, Dordrecht, The Netherlands: D. Reidel, 1988.

[14] J. G. Williams and E. M. Standish, "Dynamical Reference Frames in the Planetary and Earth-Moon Systems," chapter in *Reference Frames in Astronomy and Geophysics* (J. Kovalevsky et al., editors), Dordrecht, The Netherlands: Kluwer, 1989.

[15] C. S. Jacobs et al., "The Extragalactic and Solar System Celestial Frames: Accuracy, Stability, and Interconnection," *Advances in Space Research,* vol. 13, no. 11, pp. (11)161–(11)174, 1993.

[16] E. M. Standish, "JPL Planetary and Lunar Ephemerides, DE405/LE405," JPL Interoffice Memorandum 312.F-98-048 (internal document), Jet Propulsion Laboratory, Pasadena, California, August 26, 1998.

Chapter 3
Range and Doppler Tracking Observables

3.1 The Tracking Link

Communications from Earth to spacecraft and from spacecraft to Earth are made within internationally allocated frequency bands [1], as shown in Table 3-1:

Table 3-1. Uplink and downlink frequencies for deep-space communications.

Band	Uplink Frequency (MHz)	Downlink Frequency (MHz)
S	2110–2120	2290–2300
X	7145–7190	8400–8450
Ka	34,200–34,700	31,800–32,300

The Deep Space Network (DSN) developed S-band capability for uplinks and downlinks in the 1960s. In the mid-1970s, spacecraft were equipped with dual-frequency S/X downlinks. (Signals at the two downlink bands are coherent with each other, having been derived from the same reference signal.) In 1989, an X-band uplink capability was added. The Magellan spacecraft was the first to use this capability and could transmit coherent S/X downlinks that were derived from an X-band uplink. Most spacecraft launched in the 1990s transmit and receive at X-band only. Cassini, however, can operate with an X-band uplink and coherent X/Ka downlinks. Further use of Ka-band is planned for the 21st century. The move toward higher frequencies is largely driven by the desire for better communications performance, but higher frequencies also improve the accuracy of radiometric measurements by using shorter wave-

lengths and by reducing effects due to charged particles in the ionosphere and solar plasma.

Spacecraft range is measured by the round-trip transit time of a ranging signal generated at one of the DSN stations (located at Goldstone, California; Canberra, Australia; and Madrid, Spain). A ranging signal, consisting of a sequence of sinusoidal tones derived from the station frequency standard, is phase modulated onto the transmitted carrier signal [2]. The spacecraft receiver locks on and tracks the uplink carrier via a phase-locked loop that produces a reference signal coherent with the uplink carrier. This reference signal is used to demodulate the ranging signal, which is then passed through a lowpass filter, currently with an upper cutoff frequency of less than 2 MHz. The ranging signal is phase modulated onto the downlink carrier, a signal coherent with the uplink but offset in frequency. (For example, assuming an X-band uplink, the downlink frequency would be higher by a factor of 880/749 at X-band and 3344/749 at Ka-band.) A phase-locked loop at the receiving station produces a reference signal coherent with the received signal. This reference signal is used by the ranging assembly to demodulate the downlink signal. The received range code is compared against a model of the transmitted range code to determine the round trip transit time. Range measurements are quantized in steps referred to as range units (RU). The size of an RU depends on the frequency of the highest component of the code, and is currently about 28 cm. Doppler data are obtained by differencing the received reference signal with the station frequency reference.

A new ranging capability is being added to future flight systems. It will use a pseudo-random noise code rather than a sequence of tones. This code will be detected and regenerated onboard the spacecraft. Using this code will ensure more efficient use of the downlink power because only the range code will be modulated onto the carrier, rather than a 2-MHz noise passband, thus enabling ranging measurements to be made at greater distances and at lower signal levels [3].

Spacecraft topocentric (slant) range (see Fig. 3-1) is approximately related to the one-way signal transit time, τ_g, by the expression

$$\rho = \tau_g c \tag{3.1-1}$$

where c is the speed of light. An approximate expression for the received frequency from a spacecraft receding from Earth is

$$f_R = \left(1 - \frac{\dot{\rho}}{c}\right) f_T \tag{3.1-2}$$

where f_T is the frequency transmitted by the spacecraft and $\dot{\rho}$ is the spacecraft instantaneous slant range rate. The quantity $(\dot{\rho}/c)f_T$ is referred to as the

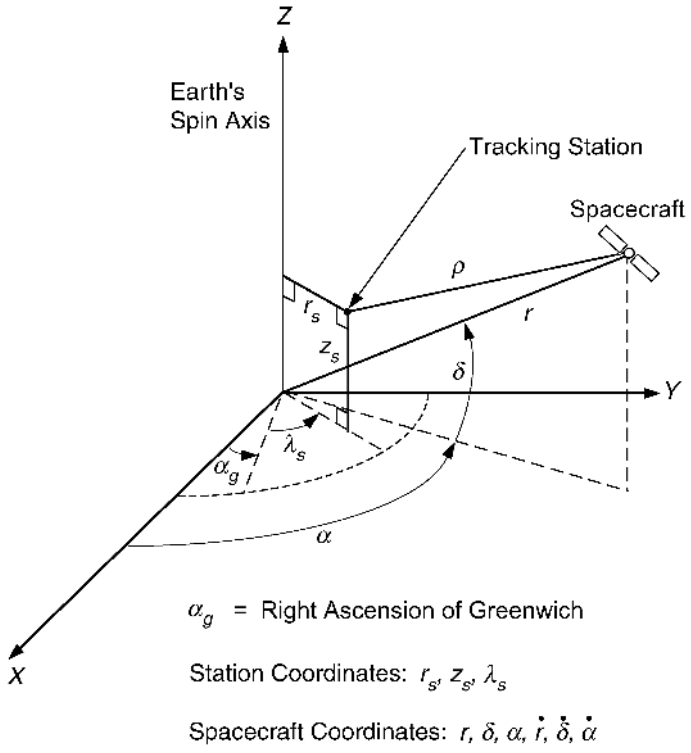

Fig. 3-1. Spacecraft and station coordinates.

Doppler shift. The Doppler measurement thus provides information on the spacecraft topocentric range rate.

A simplified illustration of the Doppler extraction process is given in Fig. 3-2. A Doppler counter measures the total phase change with resolution better than one one-hundredth of a cycle during a count time, T_c. Each time the phase of the received signal slips one cycle relative to the phase of the transmitted signal, the distance over which the signal has propagated has increased by one wavelength, or 3.6 cm at X-band. The Doppler count thus provides a measure of range change over T_c.

The most accurate ranging and Doppler measurements are obtained via a two-way tracking mode for which the transmitting and receiving stations, and hence the frequency standards, are the same. For some missions, this configuration is impossible due to the extraordinary distances. For example, the round-trip light time (RTLT) of Voyager 2 at Neptune exceeded 8 hours. In such geometries, the transmitting station can rotate out of sight of the spacecraft by the time the signal returns to Earth, and thus, a second station is

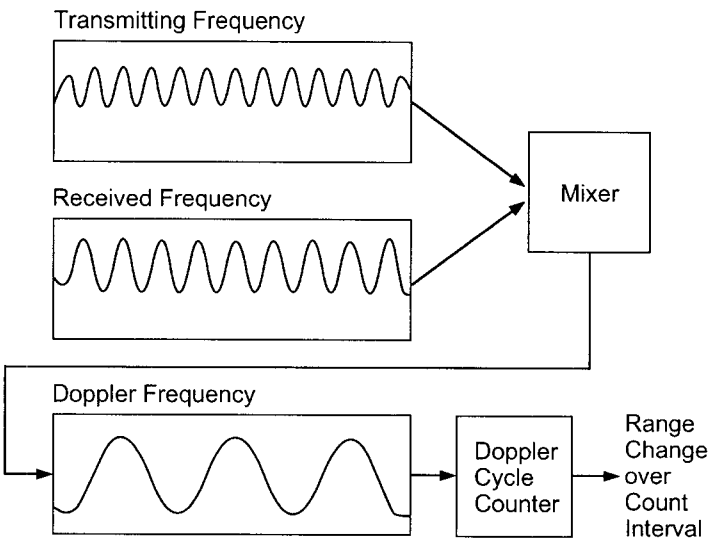

Fig. 3-2. Doppler extraction process. The difference between the transmitted and received carrier frequencies yields the Doppler tone. A cycle counter measures phase change of the Doppler tone, yielding a measure of range change during the count interval.

required to receive. This situation is referred to as three-way tracking. A third option is termed one-way tracking, in which the spacecraft generates a downlink signal from an onboard oscillator. In this mode, there is no transmission to the spacecraft.

One-way, two-way, and three-way tracking modes may be used at various times during a mission. The radiometric data obtained from each mode must be carefully modeled to account for uplink and downlink geometry, transmitting frequencies, spacecraft delays, relativistic, and other effects discernible in the residuals [4]. In the two-way mode, for example, the frequency transmitted at the spacecraft is a Doppler-shifted replica of the uplink frequency. Hence, the measured Doppler shift one RTLT later is approximately $(2\dot{\rho}/c)f_T$.

3.2 Range and Doppler Information Content

The spacecraft and station geometry at any instant of time is illustrated in Figs. 3-1 and 3-3. The slant range rate, $\dot{\rho}$, from the tracking station to a distant spacecraft can be closely approximated [5] by the expression

$$\dot{\rho}(t) = \dot{r}(t) + \omega_e r_s \cos\delta \sin(\omega_e t + \phi + \lambda_s - \alpha) \qquad (3.2\text{-}1)$$

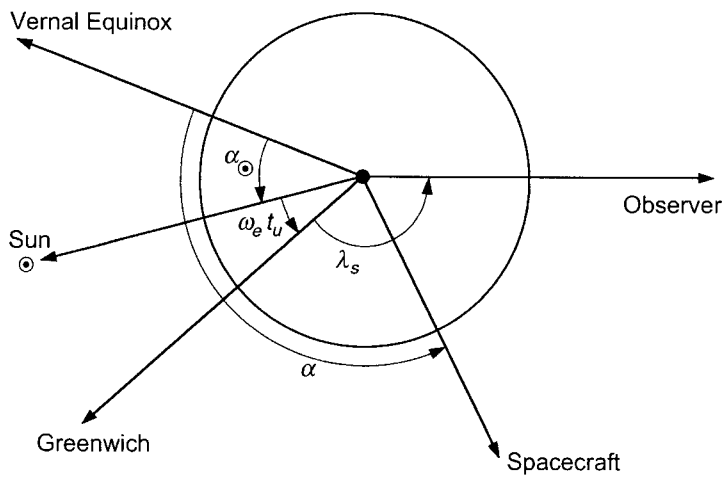

Fig. 3-3. Equatorial projection of coordinates.

where

$\dot{r}$ = geocentric range rate

ω_e = mean rotation rate of Earth

r_s = distance of tracking station from Earth spin axis

λ_s = longitude of tracking station

α = right ascension of spacecraft

δ = declination of spacecraft

ϕ = phase angle that depends on the epoch.

When time, t, is expressed as universal time (civil time at Greenwich), then ϕ is the instantaneous right ascension of the mean Sun.

As depicted in Fig. 3-4, the range rate observable given in Eq. 3.2-1 is essentially a sinusoid superimposed upon a ramp function representing the spacecraft geocentric velocity. The diurnal modulation is the result of the rotation of the tracking station about Earth's spin axis. The amplitude and phase of this modulation provide information about the spacecraft declination and right ascension. Notice, however, that accurate determination of these parameters depends not only upon the precision of the range rate observation, but also upon the accuracy to which the model parameters such as the tracking station locations and Earth orientation are known. For example, an error in station lon-

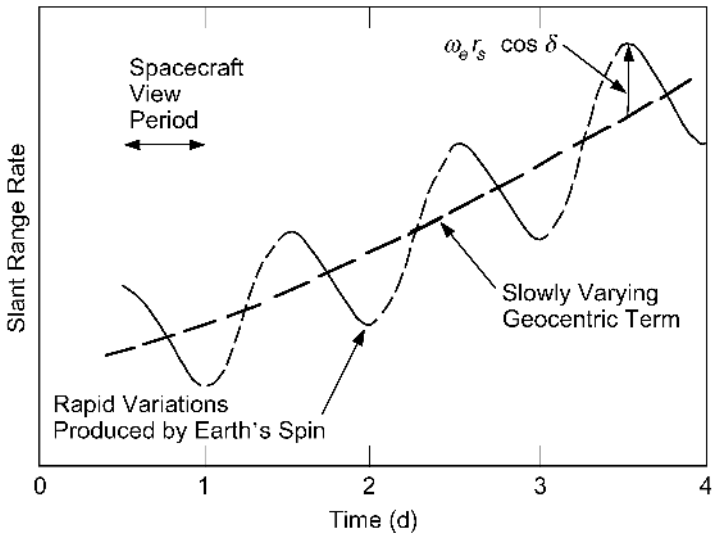

Fig. 3-4. Schematic illustration of idealized Doppler observable.

gitude maps one-for-one into an error in spacecraft right ascension. A detailed description of major Doppler modeling errors is given in the next section.

Doppler data are typically recorded continuously during the tracking pass at each DSN complex. From a single pass of Doppler, it is possible to determine spacecraft radial velocity, right ascension, and declination. Velocities normal to the line of sight can be inferred from several days or more of Doppler data [6]. Geocentric range can also be inferred from spacecraft accelerations observed in multiple passes of Doppler through constraints imposed by solar system gravitational force models.

Although orbit determination strategies have traditionally relied upon continuous Doppler passes to infer spacecraft angular position, there are significantly more powerful methods such as VLBI for measuring angles and angle rates directly. These will be discussed in Chapter 4. It should also be pointed out that range data, if continuously acquired, have a time signature similar to those for Doppler and provide spacecraft angular information as well as geocentric range and range rate. In fact, several days of continuous, biased range data with an accuracy of 1 m have the same angular information as a comparable track of Doppler with an accuracy of 0.1 mm/s.[1] The complementary information in range and Doppler observations can be useful in identifying poorly modeled spacecraft accelerations. This situation is explored further in Section 3.6.

[1]T. P. McElrath, personal communication, Navigation and Flight Mechanics Section, Jet Propulsion Laboratory, Pasadena, California, July 2000.

3.3 Tracking Data Error Sources

A number of errors in the Doppler and range observations limit the accuracy to which spacecraft orbits can be determined. For example, errors in the tracking equipment, such as clock instabilities and instrumental delays of signals, degrade accuracy. In addition, the transmission media introduce delays and dispersions into signals. Further, imperfect models of the tracking geometry, due to errors in station locations or Earth orientation, limit the ability to estimate spacecraft position. In this section, we explore the sensitivity of the Doppler and range data to current major sources of error in observable models, and we discuss means for calibrating, or removing, these errors.

3.3.1 Clock Instability

A fundamental source of error in radiometric tracking is clock instability. Consider the Doppler extraction process in Fig. 3-2. The received signal is beat against (mixed with) a local frequency reference. Any offset of this frequency reference from the actual transmitted frequency (either originating on the ground or on the spacecraft) will translate into an error in range rate. For example, in the one-way transmission mode, an oscillator onboard the spacecraft generates a reference signal that is transmitted by the spacecraft and received on the ground. The most stable space-qualified crystal oscillators currently available fluctuate about one part in 10^{13} over averaging intervals of 1000 seconds.[2] Over the longer time intervals important to navigation performance, crystal oscillator stability is generally worse. An unknown constant frequency offset of Δf relative to the nominal frequency, f, translates into a range rate measurement error of

$$\Delta\dot{\rho} = c\frac{\Delta f}{f} \tag{3.3-1}$$

As we shall see, a frequency offset larger than 10^{-13} is a major error relative to the best Doppler systems operating today. In the two-way tracking mode, the frequency standards associated with the transmitter and receiver are identical and, furthermore, a highly stable standard, such as the hydrogen maser, is typically used. These frequency standards are stable to a few parts in 10^{15} over a typical RTLT [7]. To understand how the frequency standard affects a two-way Doppler measurement, a short discussion of frequency stability is necessary.

The accepted measure of stability of frequency standards in the time domain is the two-sample Allan variance with no dead time [8]

---

[2] S. W. Asmar, personal communication, Communications Systems and Research Section, Jet Propulsion Laboratory, Pasadena, California, June 2000.

$$\sigma_y^2(\tau) = \frac{1}{2} < (\bar{y}_{k+1} - \bar{y}_k)^2 > \tag{3.3-2}$$

where $\bar{y}_k$ and $\bar{y}_{k+1}$ are adjacent measurements of fractional frequency deviation, with averaging time, τ. The brackets denote ensemble averaging. The fractional frequency deviation is computed by subtracting the clock phase error at the beginning of the averaging interval from the phase error at the end of the averaging interval, and then dividing by the product of the nominal frequency times the averaging interval. The range rate error for a count time, τ, and RTLT of $M\tau$ is given by [9]

$$\Delta\dot{\rho} = c(\bar{y}_{k+M} - \bar{y}_k) \tag{3.3-3}$$

The root-mean-square (rms) error is given by

$$c < (\bar{y}_{k+M} - \bar{y}_k)^2 >^{1/2} = \sqrt{2}\, c\sigma_y(2, M\tau, \tau) \tag{3.3-4}$$

where $\sigma_y^2(2, M\tau, \tau)$ is the two-sample Allan variance with averaging time, τ, and sample interval, $M\tau$. The Doppler error thus depends on the Allan variance at time scales of between τ and $M\tau$. Approximations of this general form of the Allan variance can be made in terms of the usual two-sample Allan variance with no dead time for several types of noise that are common for frequency standards. The DSN hydrogen masers exhibit white frequency noise at time scales of 60 to 1000 s, and they exhibit flicker frequency noise at time scales of 1000 s to about 12 hours [7]. For a Doppler count time, τ, which is less than the RTLT, which is itself less than 1000 s, the range-rate error due to frequency instability is given by

$$c < (\bar{y}_{k+M} - \bar{y}_k)^2 >^{1/2} = \sqrt{2}\, c\sigma_y(\tau) \tag{3.3-5}$$

while for a Doppler count time of τ and an RTLT of between 1000 s and 12 h, the error is approximately given by

$$c < (\bar{y}_{k+M} - \bar{y}_k)^2 >^{1/2} \approx \sqrt{2 + \log_2 M}\, c\sigma_y(\tau) \tag{3.3-6}$$

where M = RTLT/τ. The Allan standard deviation, $\sigma_y(\tau)$, of the DSN hydrogen masers is typically about 8×10^{-15} for $\tau = 60$ s,[3] and about 1×10^{-15} for $\tau = 1000$ s [7]. This effect is negligible relative to other errors in the system such as troposphere (see Section 3.3.3).

---

[3] R. L. Tjoelker, personal communication, Tracking Systems and Applications Section, Jet Propulsion Laboratory, Pasadena, California, May 2000.

Notice that for Doppler measurements, frequency stability requirements are more stringent than timing requirements. The clock epoch provides only the observable time-tag. For example, for a spacecraft in cruise, a time-tag error of 1 μs would translate into a negligible right ascension error of less than 0.1 nrad, as inferred from the Doppler signature (see Eq. 3.2-1). Doppler measurements from a planetary orbiter, such as Mars Global Surveyor (MGS), are sensitive to clock epoch at the microsecond level, however. The Doppler error $\Delta\dot{\rho}$ arising from a station clock epoch error ΔT is given by

$$\Delta\dot{\rho} = \ddot{\rho}\Delta T \tag{3.3-7}$$

Given a station clock error of 2 μs, a barely discernible Doppler measurement error of 0.016 mm/s would result for a short-period (or eccentric) orbiter accelerating at 8 m/s^2. While this size error would be difficult to detect in Doppler acquired from a single station, it could be revealed in Doppler data acquired simultaneously at two stations. Microsecond-level clock synchronization of the DSN clocks relative to UTC, routine now for about three decades, keeps this error at an insignificant level.

The effect of clock instability on two-way range data is approximately

$$\Delta\rho = \sqrt{2}\, c\tau\sigma_y(\tau) \tag{3.3-8}$$

where τ is the RTLT. With hydrogen maser stability, this effect is negligible—about 1 mm at one astronomical unit (AU) (for example, at Mars). However, clock epoch offsets between the transmitting and receiving stations can be a major error source for three-way ranging. In this case, the effect is approximately given by

$$\Delta\rho = c\Delta T \tag{3.3-9}$$

where ΔT is the clock offset. Thus, an unknown offset of 10 ns would result in a significant range error of 3 m.

The DSN has been using techniques such as observations of signals from the Global Positioning System (GPS) satellites to measure clock offsets over intercontinental distances to about the 10-ns level. Station calibrations are then required to relate tracking data time tags to station time at the clock reference point. Current calibration accuracy is about 1 μs. The GPS tracking system calibration method has the potential for near real-time clock offset measurements at the 1-ns level [10–12]. However, the navigation benefits of GPS clock calibration will be realized only if improved methods are developed to: (a) translate GPS measurement time to station time and (b) calibrate spacecraft tracking

signal path delays from the antenna front end to the baseband signal processor. The GPS calibration system is described in Section 3.4.

Although range measurements are highly sensitive to clock epoch offsets between transmitting and receiving stations, they are relatively insensitive to time-tag errors. An unknown time-tag error of ΔT would result in a range error of approximately

$$\Delta\rho = \Delta T\dot{\rho} \tag{3.3-10}$$

Thus, a time-tag error of 1 μs would result in a range error of 4 cm at a typical range rate of 40 km/s. A clock rate offset of $\Delta\dot{T}$ would result in a two-way range error of

$$\Delta\rho = c\mathrm{RTLT}\Delta\dot{T} \tag{3.3-11}$$

This effect is also small for spacecraft traveling in the inner solar system; an unknown clock rate offset of 10^{-13} causes an 11-cm range error for a one-hour RTLT.

The DSN has implemented a new frequency standard in the network, referred to as the linear ion trap standard, or LITS. This standard, when coupled with a cryogenically cooled, compensated sapphire oscillator (CSO) promises higher stability at all averaging times than the hydrogen maser [13]. Short-term stability of $3 \times 10^{-14}/\tau^{1/2}$ is achieved with the CSO, coupled with a long term stability of 6×10^{-16} or better (for $\tau > 10{,}000$ s) demonstrated by the LITS [13,14]. The first CSO will be installed at the Goldstone Deep Space Station by the end of 2000 to support the Cassini Ka-band radio science experiment [15]. Implementation at the Spain and Australia stations will be completed by the end of 2002. Once this implementation is successfully completed, the hydrogen masers will be retired from operation.[4]

3.3.2 Instrumental Effects

Limitations in station instruments arising from such factors as fundamental physics, design trade-offs, and the need for multipurpose functionality result in both random and systematic measurement errors. Random errors are caused by thermal noise, which is proportional to the receiver operating temperature and introduces a purely white noise into each measurement. Systematic errors are caused by dispersive and nondispersive instrumental delays and by antenna multipath.

The contribution of these errors to observable accuracy is highly measurement dependent. For example, group delays in the station and spacecraft elec-

[4]R. L. Tjoelker, personal communication.

tronics currently represent the major source of error in the ranging system. Uncalibrated delays of 13 ns or more in the two-way path may occur, producing biases of about 2 m in the inferred one-way range. System noise effects, on the other hand, depend largely on spacecraft transmitter power, and typically fall in the range of 10 to 100 cm with present day 2-MHz ranging systems [16].

Doppler measurement errors due to instrumentation result primarily from thermal noise and instabilities in the signal path through the receiver and exciter subsystems and the spacecraft transponder. Uncalibrated instrumental effects currently contribute about 0.003 mm/s to Doppler measurement errors for a 60-s count time.

3.3.3 Transmission Media

Charged particles in the interplanetary medium and Earth's ionosphere cause dispersive propagation delays in interplanetary radio signals. These frequency-dependent effects cause a group delay that can be closely approximated as

$$\Delta\tau_g = \frac{k}{f^2}, \quad k > 0 \tag{3.3-12}$$

Thus, a ranging code modulated on the carrier signal will experience a positive delay. Carrier phase, on the other hand, is advanced so that the phase delay is approximately

$$\Delta\tau_\phi = -\frac{k}{f^2} \tag{3.3-13}$$

The constant, k, is proportional to the total electron count (TEC) per unit area along the signal path through the ionosphere and solar plasma. The effective signal delay then depends upon the time of transmission during the Sun cycle as well as the signal ray path relative to the Sun. In addition, the ionospheric delay also varies diurnally and seasonally. The magnitude of the ionospheric effect at X-band during the daytime is approximately 20–60 cm at zenith. The nighttime effect is typically less by an order of magnitude. Furthermore, there is an elevation angle dependence that varies from a factor of one at zenith to a factor of three at the lowest elevations.

Solar plasma delays at X-band can range from 1 m to 75 m, depending largely upon how angularly nearby the Sun the signal travels. For a Sun-Earth-probe angle of 20 deg, the plasma delay at X-band typically drifts by about 1 m over an 8-h tracking pass. This effect was calculated by Kahn[5] based upon propagation observations of Woo and Armstrong [17] and Coles and

[5]R. D. Kahn, personal communication, Tracking Systems and Applications Section, Jet Propulsion Laboratory, Pasadena, California, August 1991.

Harmon [18]. Variability in solar conditions can cause the actual drift to vary by up to an order of magnitude from the mean.

The frequency dependency of charged particle delays allows for nearly complete cancellation of these effects for spacecraft with dual-frequency radio systems, for example, S- and X-band. Note, however, that this approach requires dual-frequency uplink and downlink transmissions for two-way Doppler and range tracking. Many missions operate with only a single frequency or with dual frequency only on the downlink transmission. In these cases, alternative calibration schemes are required.

One such alternative, referred to as DRVID (Differenced Range Versus Integrated Doppler), uses the equal but opposite effect on group delay and phase delay [19]. The integrated Doppler provides a measure of range change between two consecutive range measurements. The difference of these two data types yields a direct measure of the change in $2k/f^2$ between the two measurement times, thereby providing information on $\dot{k}$. Thus, DRVID provides a means for calibrating the Doppler data. Its effectiveness has been limited, however, by operational constraints and the accuracy of the DSN ranging system [20]. With present-day ranging equipment, the best one can expect is an accuracy of 40 cm over the Doppler count time.[6]

Another method for calibrating signal delays due to Earth's ionosphere involves tracking the dual-frequency L-band signals emitted by the GPS. For elevations above 10 deg, GPS calibrations of line-of-sight TEC have a root-mean-square (rms) accuracy of about 5×10^{16} el/m^2 or 3 cm at X-band [21] (see Section 3.4). After these calibrations are applied, Doppler observables at X-band contain residual fluctuations, caused by the ionosphere, of about 1 cm over 10 min.

Microwave tracking signals from deep space are also delayed by Earth's neutral atmosphere. The refractive effect of the troposphere results in approximately 2 m of signal-path delay at zenith and 20 m at 6-deg elevation. If second- and third-order effects due to bending are ignored, the tropospheric delay can be expressed as the sum of the contributions from the dry and the wet components of the atmosphere [22]. Thus, the one-way slant range correction is approximately

$$\Delta\rho = \Delta\rho_d + \Delta\rho_w \tag{3.3-14a}$$

where

$$\Delta\rho_{w/d} = z_{w/d} F_{w/d}(E) \tag{3.3-14b}$$

$z_{w/d}$ is the wet/dry zenith delay, E is the elevation angle, and $F_{w/d}(E)$ is the corresponding elevation-dependent mapping function, which is approximately given

[6] D. W. Green, personal communication, Honeywell Technology Solutions, Inc., Pasadena California, May 2000.

by 1/sin *E*. The currently preferred mapping function is credited to Niell [23]. It is acknowledged to be competitive with the best models, but has the added advantage of requiring no real-time meteorological data [24]. Tropospheric delay calibrations for radiometric data are obtained by applying the mapping function for the elevation of the ray path to an independently provided estimate of zenith delay. The dry component contributes about 95% of the total zenith delay and is proportional to the surface pressure. Under normal meteorological conditions, the dry portion is close to static equilibrium and is calculated to an accuracy of a few millimeters from measurements of surface barometric pressure, using the Saastamoinen model as improved by Elgered [24,25]. The wet portion, on the other hand, is proportional to the water vapor density along the ray path and is highly unstable [26]. Models of the static component of the wet troposphere based on local meteorological data are typically accurate to only about 4 cm at zenith [24].

Total zenith delays accurate to a centimeter or better are provided by the GPS calibration system described in Section 3.4 [27]. Once these delays are separated into wet and dry components, using surface weather data in conjunction with the Elgered model to infer the dry delay, the individual wet and dry components are mapped to the appropriate spacecraft line of sight. Zenith-delay measurement errors are magnified in this calculation by approximately 1/sin *E*, such that accuracies at 10 deg of elevation are on the order of 6 cm. More accurate calibration in the line-of-sight path delay to a spacecraft, especially at lower elevations, may require direct line-of-sight measurements such as those obtained from a narrow beamwidth water vapor radiometer (WVR) [28] or a Fourier-transform spectrometry (FTS) instrument [29].

The DSN has implemented a new generation of WVR in support of the Cassini Gravitational Wave Experiment, which is scheduled to begin in December 2001. Recent tests with two of these WVRs on the 21-km baseline at the Goldstone Deep Space Communications Complex indicate that differential atmospheric delay fluctuations can be measured to an accuracy of between 0.2 to 0.5 mm over time scales of 10 s to 10,000 s [30]. These results translate into an Allan variance that meets the Cassini stability requirements [30].

3.3.4 Platform Parameters

The quantities that define the locations of the tracking stations in the adopted inertial reference frame are referred to as platform parameters. These parameters may be divided into three distinct subsets: (a) the positions of tracking sites on Earth's crust; (b) the orientation angles of the crust relative to Earth's instantaneous axis of rotation and the equinox of date; and (c) the orientation angles of the instantaneous pole and equinox of date in the inertial reference frame.

3.3.4.1 Station Locations. The location of a DSN tracking antenna is defined as a reference point on the antenna's stationary axis [31]. For an

antenna with intersecting axes, the station location is defined as the point at which the two axes intersect. If the secondary axis is offset from the primary axis by a distance, b, the station location is defined as that point on the primary axis where the secondary axis would intersect if b were zero. These conventions give rise to model corrections to the recorded data that are carefully applied in the data analysis [4,31].

The coordinates of stations are expressed in the Conventional International Origin (CIO) 1903.0 terrestrial reference system. In this system, the z-axis is the 1903.0 standard pole. The x-axis points toward the 1903.0 meridian of Greenwich, and the y-axis completes the right-handed system, with positive y being 90 deg east. Station coordinates, as illustrated in Fig. 3-1, are defined as r_s (spin radius), λ_s (longitude measured easterly from Greenwich) and z_s (height above the equator).

It can be seen from Eq. 3.2-1 that Doppler-determined angles are highly sensitive to errors in station location components r_s and λ_s. A longitude error maps one-for-one into spacecraft right ascension, while an error in r_s results in a spacecraft declination error of

$$\Delta\delta = \frac{\Delta r_s}{r_s} \cot \delta \tag{3.3-15}$$

Since the planetary orbits about the Sun lie very nearly in the ecliptic plane, this error can be approximated as

$$\Delta\delta > 2\frac{\Delta r_s}{r_s} \tag{3.3-16}$$

Thus, an error of 5 cm in r_s translates into an error of at least 20 nrad in the Doppler-inferred declination.

Since the early 1980s, the vectors between many of the DSN stations (that is, the relative station locations) have been precisely determined by VLBI measurements of natural radio sources (see Chapter 4). Vector baselines have been determined to about 2 cm [32]. Changes in baseline lengths of a few centimeters per year have been measured to an accuracy of 1 to 2 mm per year [33].

The VLBI measurements provide accurate information on relative station positions, but must be coupled with other measurement techniques in order to tie the locations to the geocenter. Data from GPS and satellite laser ranging (SLR) are sensitive to geocenter location through the satellite dynamics. These data provide estimates of station locations accurate to the centimeter level [34,35]. Folkner [36] has utilized available VLBI, GPS, and SLR station location estimates, together with precise local surveys between collocated stations, to determine a subset of DSN station locations accurate in a geocentric reference frame to 3 cm, or better, in each component. Locations of newer DSN antennas were determined to an accuracy of 5 to 9 cm, using a combination of

GPS measurements and conventional survey. With additional effort in the local survey, these stations could also be located to the centimeter level, if such accuracy were required. The locations are given in the International Terrestial Reference Frame ITRF93, a frame consistent with Earth-orientation calibrations delivered to navigation teams [35,36]. Measurements of continental drift provided by VLBI and/or GPS permit the needed corrections for station motion since the 1993 epoch [36]. Corrections are also made for the effects of solid Earth tides, ocean loading, and pole tide, which are significant at the centimeter level [4].

3.3.4.2 Earth Orientation. The orientation of the terrestrial reference frame relative to the instantaneous axis of rotation and the equinox of date can be defined by three quantities, commonly referred to as X and Y pole location parameters and UT, or UT1 – UTC, a correction to time of day. The Y parameter is a right-handed rotation about the x-axis of the 1903.0 CIO frame. The X parameter is a subsequent rotation about the y-axis. The UT correction is then applied to compute the Greenwich hour angle of the true equinox of date [4,31]. The X and Y polar motion parameters are also referred to as PMX and PMY, respectively.

Polar motion, the motion of the solid Earth with respect to Earth's spin axis, has been measured for more than 100 years. It consists principally of circular oscillations with amplitudes of 100 and 200 mas (milliarcseconds) and periods of about one year and 433 days, respectively. In addition, there is a long-term drift of a few milliarcseconds per year. Decade time-scale variations have also been observed with amplitudes of 50 mas [37]. Rapid polar motion, fluctuating on time scales of a few weeks to a few months, has been measured with peak-to-peak variations of less than 20 mas [38]. The total effect of these variations produces excursions in the pole location of 10 m over a period of one year [39] as illustrated in Fig. 3-5. Oscillations on time scales of a year or less are believed to be driven by the atmosphere and oceans [40], while the Chandler wobble (433-day period) is possibly also excited by the atmosphere and oceans [41]. The long-term drift may be due to postglacial rebound or to melting ice in Greenland or Antarctica [42].

Earth's rate of rotation is not constant. The length of day (LOD) varies by several milliseconds over a wide range of time periods. Variations over a period of one year are illustrated in Fig. 3-6. Secular increases in LOD of about 1 ms per century are attributed to tidal dissipation of lunar forces. There are also secular effects produced by changes in the moment of inertia of the solid Earth due to the melting of ice following the ice ages [43]. Variations up to 5 ms in LOD over decadal and interannual time scales are believed to be primarily due to angular momentum transfer between Earth's solid mantle and fluid core [43]. Rapid variations on time scales of less than two years have been

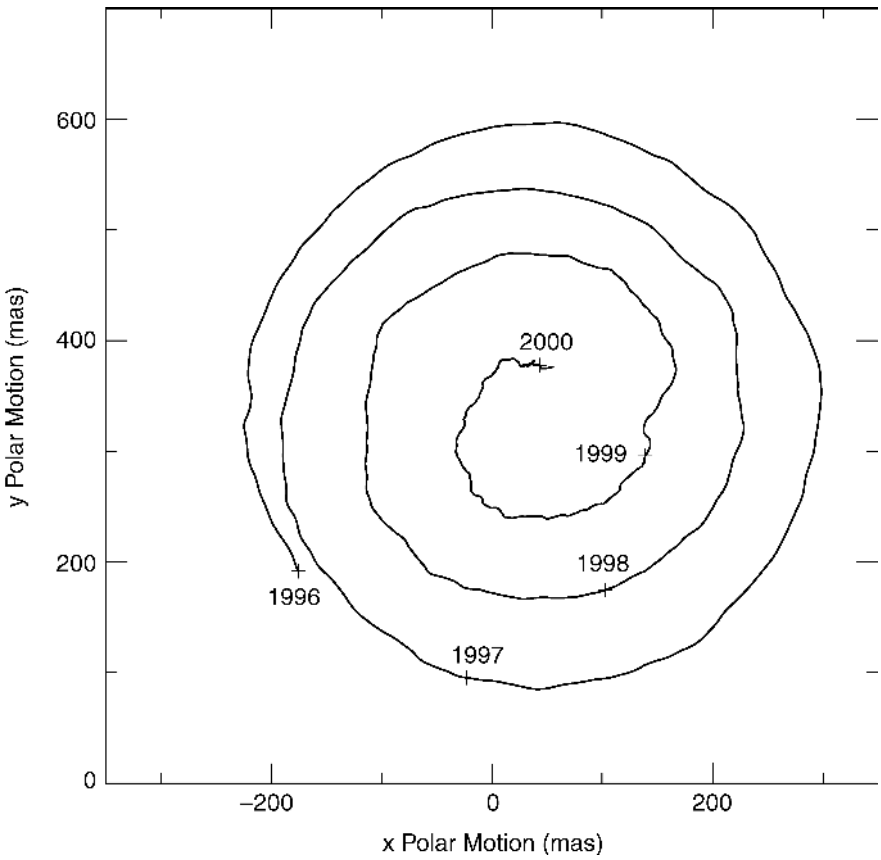

Fig. 3-5. Observed values of polar motion from January 1996 to January 2000.

shown to be highly correlated with atmospheric effects [44]. In fact, atmospheric angular momentum (AAM) data are used by the DSN to assist in determining Earth rotation time series [45].

If left uncorrected in the tracking observable models, UT and polar motion (PM) errors translate directly into spacecraft angular position errors. For example, an error of 1 ms in UT produces an error of about 70 nrad in spacecraft right ascension as determined from a single pass of Doppler data (see Eq. 3.2-1). This level of error corresponds to about 16 km at Mars.

Flight project requirements for UT and PM calibration accuracy are typically stated in terms of displacement at Earth's surface. The two polar motion parameters, PMX and PMY, have a conversion of about 3 cm per mas of rotation. The UT parameter is given in milliseconds where 1 ms translates to 46 cm of rotation at the equator.

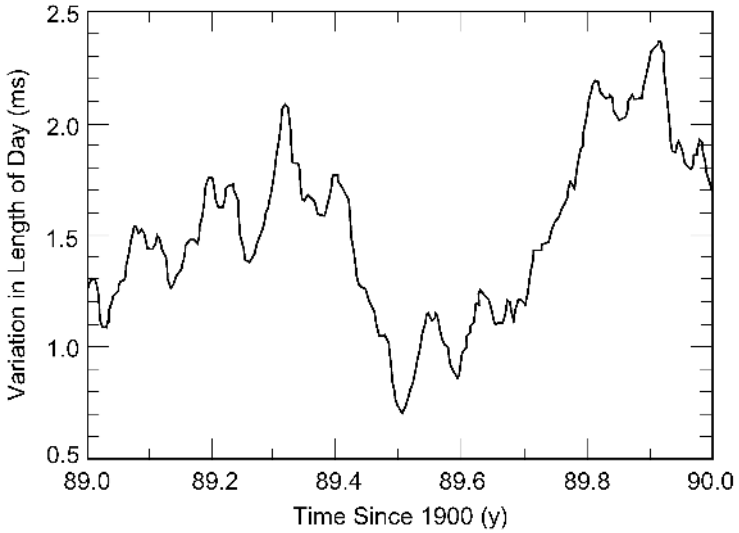

Fig. 3-6. Sample length-of-day time series.

Flight project requirements for UT and PM calibration accuracy have become more stringent during the last two decades. The Galileo Project required 30-cm prediction accuracy per component over a week, and 10-cm accuracy three weeks after the observations [46]. Mars Pathfinder, on the other hand, required 10-cm prediction accuracy over a week and 5-cm accuracy three weeks after the observations [47]. It is anticipated that a number of future projects will require near-real-time accuracies of 10 cm or better in each component.

Due to the stochastic nature of these effects and the need to calibrate navigation data in near-real time, it is necessary to generate a time series for PMX, PMY, and UT, predicting well into the future. This time series is calculated using the Kalman Earth Orientation Filter (KEOF), a program that incorporates state-of-the-art geophysical models, precise measurements from a variety of observation techniques, and stochastic models for the UT and PM parameters [48]. Measurement techniques used include the GPS, SLR, VLBI, AAM, and lunar laser ranging (LLR) [45,49].

The GPS Calibration and Tracking System (see Section 3.4) provides near-continuous measurements of PM and LOD. The epoch values of UT required for integrating the LOD measurements are obtained primarily from VLBI, and as available, from LLR. The SLR data provide additional PM estimates, while daily AAM are a good proxy for LOD. Furthermore, the AAM 5-day forecasts, obtained from numerical weather models, are valuable for generating predictions of LOD [45].

Time series from these sources are typically referenced to an internationally recognized terrestial reference frame (at present ITRF97) [34]. However, as noted in Section 3.3.4.1, navigation currently expects to receive all platform parameters referenced to ITRF93 in order to maintain consistency with the station location file now in use. Therefore, prior to KEOF processing, each of the input series is rotated, as necessary, to ITRF93.

Time series of UT and PM produced with the KEOF in the ITRF93 reference frame are delivered twice per week to navigation, with a latency of approximately one day past the data arc. During critical mission phases, deliveries may be required every day, as was the case for Mars Polar Lander during the week leading up to its scheduled encounter in 1999. These rapid-service time series, when used for near-real-time calibration on the delivery day, have one-sigma accuracies of 3 to 5 cm in PM, and 7 cm in UT. Accuracy of the predicted values degrades with time, and by 7 days, these values are 11 to 13 cm for PM and 24 cm for UT (see Fig. 3-7). After-the-fact calibrations with a 2-week delay have accuracies as good as 4 to 6 mm in each component, due to the abundance of high-quality prior measurements.[7]

Accuracies of the various time series are assessed based upon comparisons with truth series referred to as SPACE98, SPACE99, etc. [50–52].These time series are generated once per year, using the final "best" products of the various space geodetic data sources. The reference series SPACE98 is purported to have an accuracy over the last several years approaching 2 mm in each PM parameter and 6 mm in UT [51].

3.3.4.3 Precession and Nutation. The effects of lunar and solar gravitation on an oblate Earth cause the orientation of Earth's spin axis to continually change with respect to inertial space. These changes in orientation are described by a long-period rotation of the spin axis, referred to as precession, upon which is superimposed a small periodic oscillation known as nutation. Models for precession and nutation are used to rotate from "of date" coordinates at a measurement epoch to the celestial reference frame and associated epoch used by navigation to calculate spacecraft orbits. The nutation model adopted by the IAU in 1980, and used for interplanetary navigation, is deficient at about 3 to 4 mas per year [53]. A revision to this model by Mathews et al.[8] is purported to have an accuracy of 0.15 mas, based upon comparisons to VLBI observations. The new model was adopted by the IAU in August 2000.

---

[7] R. S. Gross, personal communication, Tracking Systems and Applications Section, Jet Propulsion Laboratory, Pasadena, California, April 2000.

[8] P. M. Mathews, T. A. Herring, and B. A. Buffet, "Modeling of Nutation-Precession: New Nutation Series for Nonrigid Earth, and Insights into the Earth's Interior," submitted to the Journal of Geophysical Research, 2000.

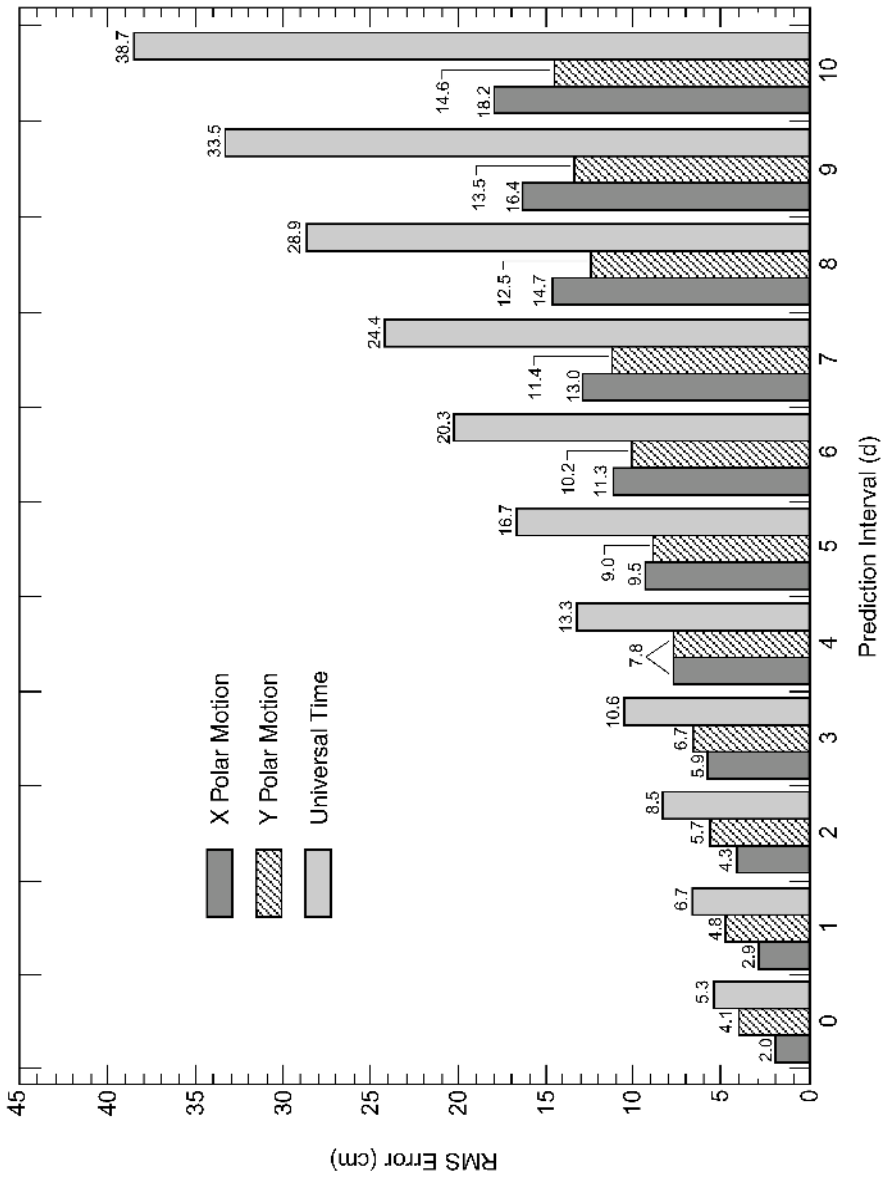

Fig. 3-7. Errors in predicted values for polar motion and universal time as a function of prediction interval past last measurement.

Corrections to the precession and nutation models used for interplanetary navigation are obtained from VLBI observations of natural radio sources [33,54]. These corrections are provided to navigation in ICRF93 (see Section 2.2), a radio reference frame consistent with ITRF93. Precession and nutation models that incorporate these corrections are accurate to 5 nrad up to a year beyond the VLBI observations [55].

The rotations for precession and nutation, following the rotations for UT and PM, yield station coordinates in the radio reference frame. A final small correction may then be required to rotate to the ephemeris frame used for navigation (see Section 4.1.3) [4].

3.4 The GPS Calibration and Tracking System

Calibration of DSN tracking data for media delays, Earth orientation, and clock offsets is largely dependent upon data from the GPS. This system consists of at least 24 satellites spaced around the globe in six orbit planes at a geocentric altitude of approximately 26,000 km. Each satellite continuously transmits dual L-band carriers (L1 = 1.2276 GHz and L2 = 1.57542 GHz) modulated with a pseudorandom noise code (P-code) from which properly equipped receivers can measure precise range and range change [56,57]. The range data are referred to as pseudorange, due to an embedded unknown clock offset between the GPS transmitter and the receiver. These clock offsets are typically modeled and accounted for in the data analysis [58,59]. Range change information is obtained from measurements of the carrier phase.

GPS satellite orbits are chosen to ensure that ground-based observers can simultaneously receive signals from at least four satellites at all times [56,57]. In reality, visibility typically is such that it is possible to receive signals from more than four satellites. Receivers designed for the high-performance applications described in this monograph are capable of concurrently tracking at least eight satellites [60]. It is this abundance of simultaneous high-precision multisatellite measurements at multiple sites that gives the GPS tracking approach its remarkable power.

GPS transmissions are under the jurisdiction of the U.S. Department of Defense (DoD). For security reasons, the DoD has implemented a number of measures designed to limit user point-positioning accuracy. These measures include encrypting (referred to as antispoofing) the precise ranging codes modulated on L1 and L2 and dithering (known as selective availability [SA]) the transmitter clocks [57]. Under SA, coarse accuracy (50 to 100 m) point positioning can be obtained with a single frequency receiver tracking the clear acquisition (CA) code modulated on L1 [61]. In the absence of SA, a user can achieve point positioning accuracy of 5 to 15 m, depending largely on corrup-

tion due to the ionosphere. As of this writing, the DoD has elected to turn off SA, a move that will significantly benefit civil GPS users.

Meanwhile, civil users with high-accuracy requirements have developed a number of means for addressing DoD security measures. These measures include codeless techniques for acquiring precise dual-frequency range and carrier phase [62–64], differential techniques or explicit clock estimation to eliminate SA effects, and utilization of ground networks to generate high-accuracy satellite orbits [59,65]. The application of these and other techniques since the early 1990s has enabled differential, stationary positioning over intercontinental distances to an accuracy of 1 cm or better [66]. Precise orbit determination for the TOPEX/Poseidon satellite, carrying a dual-frequency GPS receiver, was demonstrated in nonreal time, with an accuracy of better than 3 cm in altitude and 5 cm in the cross-track and down-track components [67]. Recent development of wide-area differential GPS systems has led to real-time transfer of GPS orbit and clock corrections to users over satellite links [68,69]. This capability will permit dual-frequency users with appropriate on-board processing capability to obtain global, instantaneous positioning with horizontal accuracy of 10 cm and vertical accuracy of 20 cm [70,71].

A major element in each of these exceptional achievements has been the use of globally distributed, geodetic-quality GPS ground receivers. The International GPS Service (IGS), a multinational organization of more than 75 contributing agencies, currently coordinates the operation of a global GPS network of approximately 200 ground receivers and seven analysis centers [72,73]. The IGS Central Bureau and one of the analysis centers are located at the Jet Propulsion Laboratory (JPL). The IGS provides tracking data, GPS satellite orbits, and other data products to a worldwide community of researchers and other users. This tracking network includes a subnet of receivers located at each DSN complex as well as the Global GPS Network (GGN), a 60-site network implemented and operated by JPL for the NASA Solid Earth and Natural Hazards Program [72]. Data from a global subset of the GGN and from the DSN are returned in a continuous stream, with latency of a few seconds, to the GPS Data Handling Facility at JPL. Latency varies for the other IGS sites, with 75% of the sites having data available within 6 hours [72].

Receivers in the IGS network are capable of codeless operation and can concurrently track at least eight satellites. A number of receivers installed since 1998 are capable of 12-satellite tracking [60]. Typical rms accuracies of the dual-frequency-combined (that is, "ionosphere-free") measurements are 5 mm in carrier phase and 50 cm in pseudorange when operating in the codeless mode [66]. These accuracies are sufficient to meet the requirements for DSN tracking-data calibrations [59].

Calibration accuracy requirements for navigation tracking data can be satisfied with GPS data from at least 12 sites having uniform global distribution

[59,74]. An automated GPS calibration system has been implemented by the DSN to process on a daily basis all available data acquired during the preceding 27 hours from approximately 21 stations. These 21 sites include receivers at each DSN complex and a globally distributed subset of the IGS network. Calibrations are generated on 5-minute time intervals and are made available in tabular form within 12 hours after the last data are recorded.

The GPS calibration system utilizes dual-frequency range and carrier-phase measurements from the 21 sites to determine GPS orbits, Earth orientation, offsets between clocks, site-dependent tropospheric delays, and a number of other secondary parameters [59]. These calculations are performed with Gipsy-Oasis II, a least-squares estimation program developed for high-accuracy geodesy and satellite orbit determination [75]. The estimated Earth orientation parameters are PMX, PMY, and LOD. An unambiguous value for UT cannot be obtained from GPS alone, since a rotation of the stations in longitude cannot be distinguished from a corresponding rotation of the satellite constellation. However, data from VLBI provide monthly, unambiguous measurements of UT to an accuracy of 0.02 ms (0.9 cm) [52,76]. The GPS calibrations are tied to the ITRF97 [34,76], through the use of six fiducial stations whose locations are held fixed at the ITRF97 values in the least-squares filter. Table 3-2 gives the accuracies of these calibrations.

Table 3-2. Accuracies for the GPS rapid-service calibrations.

Physical Parameters	Calibration Accuracy
Earth orientation, PMX, and PMY	0.3–0.4 mas (1 cm) [77]
LOD	0.03 ms (1.4 cm)[a]
Zenith troposphere delay	< 1 cm [78]

[a]R. S. Gross, personal communication.

This performance enables the timely delivery of KEOF files and troposphere files at the requisite accuracy for navigation (see Sections 3.3.4.2 and 3.3.3).

Clock offsets between GPS receivers at DSN sites are estimated in the daily rapid-service processing to a precision of 100 psec [77]. However, embedded in these estimates are differential delays through the GPS antennas, cabling between those antennas and the GPS receivers, and more significantly, the GPS receiver electronics. Tests performed in 1989 demonstrated that these delays could be calibrated to better than 1 ns through such procedures as zero-baseline tests and traveling clocks.[9] Moreover, variations in these delays can

[9]L. E. Young, personal communication, Tracking Systems and Applications Section, Jet Propulsion Laboratory, Pasadena, California, May 2000.

be controlled to well below 1 ns by the use of quality cabling and a thermally controlled environment for the receivers [79]. It is therefore possible to implement the capability for determining intercomplex clock offsets to an accuracy of 1 ns or better. However, the current tie between the GPS receiver clock and the local station clock to which spacecraft tracking is referenced is not good to this level, and path delays through the instrumentation used for spacecraft tracking are not calibrated to this level. The GPS calibration system, with proper links to the station clocks, would be capable of delivering nanosec inter-complex timing information for navigation should a requirement for this capability materialize. The current GPS rapid-service calibration system could make clock synchronization information available on a daily basis. In addition, the advent of real-time GPS data retrieval and processing suggests the future possibility of nanosecond-precision clock synchronization in near-real time [70]. However, in order to realize the full navigation benefits of this timing information, it will be necessary to improve calibration accuracy for instrumental path delays in the spacecraft tracking equipment. Today, for example, station instrumental path delays can only be calibrated to this level by observations of natural radio sources. Since instrumental delays vary with time, it is necessary to perform these calibrations at the time of radiometric measurements.

Dual-frequency measurements from GPS satellites are also used to calibrate spacecraft signals for ionospheric delays. The P2−P1 observable, derived from pseudorange measurements of the P-code on the L1 and L2 downlinks, provides an absolute measure of the ionospheric delay between the receiver and satellite, but contains more multipath and system noise than the carrier-phase data. The differenced pseudorange measurements also contain biases due to interfrequency delays in receiver and satellite hardware. These delays are nearly constant over several days and can be estimated or separately calibrated [80,81]. The L1−L2 phase-based observable provides a more precise measure of the ionospheric delay, but contains an unknown bias resulting from carrier-cycle ambiguity. The combination of these measurements yields a highly precise time history of TEC along the line of sight to each GPS satellite.

Calibrations for deep space tracking signals require the application of an algorithm to map the TEC values obtained from the GPS measurements to the appropriate spacecraft line of sight. As currently implemented, the algorithm assumes that the ionosphere can be represented as a single thin shell located at an altitude of 450 km above Earth's surface. TEC measurements between the GPS satellites and each DSN complex are used to determine the local shell characteristics, from which ionospheric delays to a particular spacecraft line of sight are calculated. Accuracy of this local thin-shell approach has been assessed at approximately 5 TEC units (TECU) (or 3 cm at X-band) for DSN tracking of spacecraft above 10 deg elevation [21]. Accuracy can be as good as

3 TECU at moderate to high elevations and as bad as 7 to 8 TECU below 10 deg [21].

A global ionosphere mapping technique, referred to as GIM, is under development and promises to provide a more robust and accurate method for spacecraft calibration [21,82–84]. GIM utilizes worldwide TEC measurements from IGS network data to characterize a global ionosphere having three layers [85]. When GIM is fully operational (circa 2002), accuracies of DSN ionospheric calibrations are expected to improve by as much as a factor of two for spacecraft at low-elevation angles. Thus, calibration accuracies of 3 to 5 TECU should be achieved over the entire range of elevation [83,85].

3.5 Range and Doppler System Measurement Performance

The effects of all significant measurement errors on range and Doppler tracking observables have been described in previous sections. These error sources are summarized in Table 3-3. The evolution of tracking capabilities is illustrated by estimating system performance for three cases: (a) 1980 radiometric tracking at S-band, (b) the 1992 system operating at X-band, and (c) the current (2000) system operating at X-band. Error contribution due to thermal noise depends on spacecraft telecommunication parameters and is a function of the distance from the tracking station to the spacecraft; typical values are given in Table 3-3.

Tracking at a single-frequency band in the two-way mode has been assumed for each case. Dual-frequency downlinks, which are available from some spacecraft, can be used to reduce the effects of the ionosphere and solar plasma. For example, solar plasma delays exceeding 200 m in S-band Viking Lander range measurements were calibrated to about 8-m accuracy using dual S and X downlinks from the Viking orbiters [86,87]. Today, spacecraft operate primarily with an X-band uplink and downlink. Plasma effects for an X-band two-way link are reduced by a factor of 13 when compared to an S-band link. Future use of Ka-band two-way links would reduce this effect by an additional factor of 14.

For the current system, the random error of 0.03 mm/s for an X-band Doppler measurement made over 60 s is due primarily to fluctuations in solar plasma density along the line of sight. This value varies with proximity of the ray path to the Sun and with the solar cycle. The random error for a range measurement is due primarily to thermal noise.

A range observable, being an absolute measure of distance, is sensitive to measurement biases as well as random errors. For moderate Sun-Earth-probe angles, the accuracy of the current system is limited by knowledge of delays through station and spacecraft electronics. This instrument bias is about 2 m.

Table 3-3. Radiometric measurement system error characteristics.

Error Source	Magnitude		
	1980 S-Band	1992 X-Band	2000 X-Band
Random error for 60-s average			
Doppler	1 mm/s	0.03 mm/s	0.03 mm/s
Range	200 cm	60 cm	60 cm
Instrument bias (range)	5 m	5 m	2 m
Instrument stability @ 8 h	10^{-13}	10^{-14}	10^{-14}
Station locations			
Spin radius	100 cm	10 cm	3 cm
Longitude	100 cm	10 cm	3 cm
Baseline components	30 cm	5 cm	2 cm
Earth orientation (1-d prediction)	100 cm	30 cm	7 cm
Earth orientation (after the fact)	20 cm	3 cm	1 cm
Troposphere			
Zenith bias	4.5 cm	4.5 cm	1 cm
Line-of-sight fluctuation (over 10 min at 15-deg elevation)	1 cm	1 cm	1 cm
Ionosphere (line of sight, above 10 deg)	100 cm	3 cm	3 cm
Solar plasma			
20-deg Sun-Earth-probe angle			
Total line of sight	229 m	17 m	17 m
Drift over 8 h	15 m	115 cm	115 cm
Station-differenced	7 cm	0.5 cm	0.5 cm
180-deg Sun-Earth-probe angle			
Total line of sight	16 m	116 cm	116 cm
Drift over 8 h	2 m	15 cm	15 cm
Station-differenced	1 cm	0.1 cm	0.1 cm
Station clock			
Epoch	1 μs	1 μs	1 μs
Rate	10^{-12}	5×10^{-14}	5×10^{-14}
Stability @ 1000 s	10^{-14}	10^{-15}	10^{-15}

Antenna multipath, media fluctuations, and instrumental delay variations introduce systematic effects over time scales varying from seconds to hours, but the magnitudes of these effects are less than the instrument bias by a factor of at least two [88].

Doppler performance for navigation is assessed by looking at the accumulation of range error over a station tracking pass. The current system error with the largest magnitude is due to fluctuations in solar plasma delay along the line of sight. At X-band, the plasma delay drift over an 8-h pass varies from as little as 1 m at solar opposition to 20 m or higher at Sun-Earth-probe angles of 20 deg or less. But this error, being of random signature, may not degrade the spacecraft state estimate as seriously as the more systematic, few-centimeter-level errors that arise from uncertainties in platform parameters.

3.6 Range and Doppler System Positioning Performance

For the last several decades, navigation has relied primarily upon the Doppler and range systems for Earth-based tracking [89]. As previously noted, several days of Doppler are sufficient to determine an interplanetary orbit, at least in benign geometries and well-modeled force fields. Unfortunately, there are situations where Doppler tracking alone can lead to erroneous estimates of spacecraft position. For example, determination of spacecraft declination from a 12-h pass of Doppler, weighted at 0.1 mm/s, is typically accurate to about 50 nrad to 100 nrad for $\delta = 23$ deg [90]. However, the sensitivity of a single Doppler pass to errors in declination is proportional to sin δ, which vanishes at $\delta = 0$ (see Eq. 3.2-1). Thus, as a spacecraft passes through zero declination, a longer Doppler arc is needed, or tracking must be supplemented with an alternative technique for measuring angles [91,92]. Long arcs of Doppler and range data can, under favorable conditions, provide angular position accuracy of 40 nrad or better [55].

Determination of spacecraft angular position from Doppler and range data may also be severely degraded by inaccurately modeled forces such as spacecraft gas leaks, thruster firings, or solar radiation pressure. These forces are difficult to model since they are influenced by unknown, but significant, stochastic terms [93]. The integrity of the modeling is important because range, right ascension, and declination are not directly measured by the Doppler observable, but instead are weakly determined from signatures in the observables. For example, any unmodeled effects that alter the amplitude and/or phase of the diurnal signature in the data may be interpreted by the estimator as changes in spacecraft declination and/or right ascension (see Eq. 3.2-1). Moreover, these inferred changes may be quite large relative to actual perturbations

in the trajectory induced by the unmodeled forces. Consider, for example, the simplified example [94] shown in Fig. 3-8. In this example, a 5-m perturbation in range to the spacecraft is interpreted by the estimator as a 1000-km shift in the lateral, or plane-of-sky, position. In this case, the estimator is constrained by dynamical models to straight-line motion. The unmodeled accelerations cause a deviation from the modeled path of 5 m in the geocentric range direction. The estimator, given precise knowledge of geocentric range and constrained to straight-line motion, will adjust the value of the less-certain lateral position parameter in order to minimize the data residuals. Since the angular position parameters are weakly determined from the Doppler and range data, large changes in these parameter values may be required to reduce the data residuals and remove the observed signature. In the cited example, a range change of 5 m at a distance of 10^8 km translates to 1000 km in plane-of-the-sky displacement.

This hypothetical example illustrates the sensitivity of weakly determined parameters to mismodeled forces and demonstrates that solving for the orbit parameters from Doppler and range data alone can be highly risky. As this example shows, large errors in weakly determined position parameters can result from unmodeled forces on the spacecraft, particularly if those forces move the spacecraft in a direction that is well-determined. Specifically, erroneous force models conspired with precise range knowledge to produce a large and incorrect displacement in the estimate of spacecraft angular position. This example also illustrates the frequently encountered discrepancy between orbits

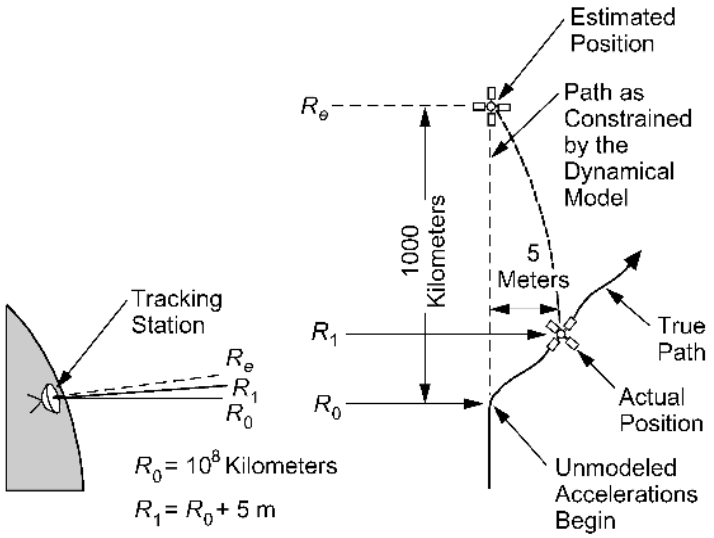

Fig. 3-8. Illustration of orbit-determination errors resulting from mismodeled dynamics, poorly measured angles, and the use of precise ranging.

determined with Doppler only and those obtained from Doppler and precise range measurements. Ironically, in the presence of mismodeled forces, less accurate or no range data can result in a more accurate orbit estimate [95]. The optimum resolution to this dilemma is not the deweighting or discarding of the range data, but rather the incorporation of appropriate stochastic models for spacecraft motion into the data-analysis software. Sequential least-squares filters have been successfully applied to estimation problems of this type for more than two decades [96]. These filters effectively deweight the dynamic constraints by allowing stochastic accelerations to be modeled and estimated. But the key to obtaining highly accurate orbit solutions is the proper utilization of data that provide a direct and accurate measure of all three components (r, α, δ) of spacecraft position.

These three components of position can also be measured using only the DSN ranging system. Simultaneous reception of ranging signals from two complexes during view period overlaps can provide a measure of angular position. This data type is referred to as differenced two-way and three-way range and is illustrated in Fig. 3-9. Differenced range was developed for the Voyager mission as a means of measuring declination to an accuracy of 1 μrad at the Saturn low-declination encounters [89]. The limiting errors for these observables are uncalibrated biases due to clock offsets and different instrumental delays at the two stations, currently as high as 1 μs (300 m). The required 6.4-m differenced range accuracy (equivalent to 600 nrad on the Goldstone-to-Canberra baseline) was

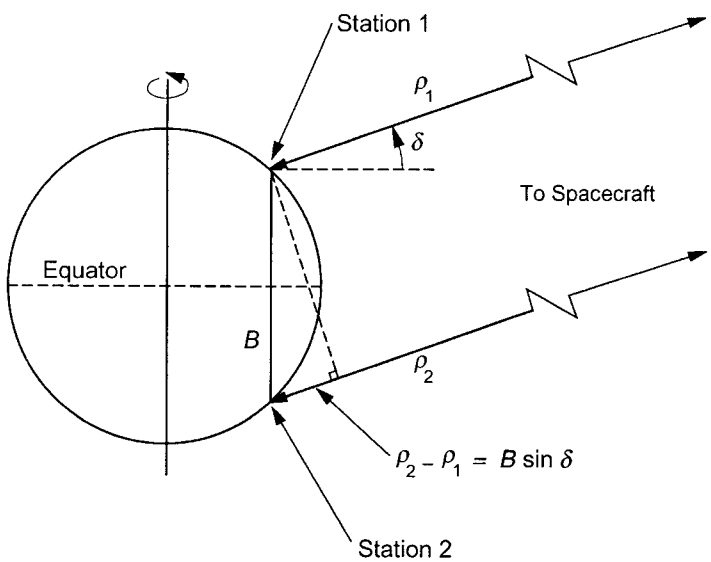

Fig. 3-9. Differenced simultaneous range from two stations, providing a measure of spacecraft angular position.

achieved instead with differenced near-simultaneous two-way range [95]. This data type is operationally difficult due to the round-trip light time and the uplink handover from one station to another. Furthermore, as the time between two-way measurements increases, the differenced observables are increasingly contaminated by uncalibrated space plasma and other line-of-sight delay variations. These problems were especially acute for the Voyager S-band ranging system, and following the Saturn encounter, the project decided to no longer acquire near-simultaneous range data [95].

Analysis in the early 1990s of two-way range and Doppler (S-band uplink and X-band downlink) data from the Ulysses spacecraft just prior to the Jupiter encounter suggested that range accuracies of a few meters were achievable [97]. This analysis also indicated that observations of this quality from two or more DSN complexes could provide spacecraft declination to 200 nrad in low declination (4 to 8 deg) situations. Improvements in range calibrations (see Table 3-3) have enabled some reduction in these angular errors. However, future missions requiring high-accuracy (50 nrad, or better) angles from Earth-based tracking will rely upon VLBI technology.

For a planetary orbiter, the motion of the spacecraft about the planet induces a strong signature in the Doppler received at Earth. The planet-relative position of the spacecraft may be recovered from analysis of this signature over one or more revolutions. However, the orientation of the orbit plane about the line of sight from Earth to the planet is not determined as accurately as the other components of state. This orientation component may be directly observed by either Doppler data acquired simultaneously at two stations and then differenced, or by interferometric delay-rate measurements [98]. For two spacecraft in orbit about the same planet, which may be observed simultaneously in the same beamwidth of Earth-based tracking antennas, differential measurements may dramatically improve orbit accuracy for both spacecraft, as discussed in Chapter 5.

References

[1] N. F. deGroot, "Radio Frequency Selection and Radio Interference Prevention," chapter in *Deep Space Telecommunications Systems Engineering* (J. H. Yuen, editor), New York: Plenum Press, 1983.

[2] J. C. Breidenthal and T. A. Komarek, "Radio Tracking System," chapter in *Deep Space Telecommunications Systems Engineering* (J. H. Yuen, editor), New York: Plenum Press, 1983.

[3] J. B. Berner et al., "Regenerative Pseudo-Noise Ranging for Deep Space Applications," *TMO Progress Report 42-137,* vol. January–March 1999,

http://tmo.jpl.nasa.gov/progress_report/issues.html Accessed October 16, 2000.

[4] T. D. Moyer, *Formulation for Observed and Computed Values of Deep Space Network Data Types,* JPL Publication 00-7, Jet Propulsion Laboratory, Pasadena, California, October 2000.

[5] T. W. Hamilton and W. G. Melbourne, "Information Content of a Single Pass of Doppler Data from a Distant Spacecraft," *Space Programs Summary 37-39, Vol. III, The Deep Space Network,* Jet Propulsion Laboratory, Pasadena, California, pp. 18–23, May 31, 1966.

[6] D. W. Curkendall and S. R. McReynolds, "A Simplified Approach for Determining the Information Content of Radio Tracking Data," *Journal of Spacecraft and Rockets,* vol. 6, no. 5, pp. 520–525, May 1969.

[7] P. F. Kuhnle, "NASA/JPL Deep Space Network Frequency and Timing," *Proceedings of the Twenty-first Annual Precise Time and Time Interval (PTTI) Applications and Planning Meeting,* Redondo Beach, California, pp. 479–490, November 28–30, 1989.

[8] J. A. Barnes et al., "Characterization of Frequency Stability," *IEEE Transactions on Instrumentation and Measurement,* vol. IM-20, no. 2, pp.105–120, May 1971.

[9] J. S. Border and E. R. Kursinski, "Deep Space Tracking and Frequency Standards," *Proceedings of the IEEE 45th Annual Symposium on Frequency Control,* IEEE 91CH2965-2, Los Angeles, California, pp. 594–607, May 29–31, 1991.

[10] C. E. Dunn, S. M. Lichten, D. C. Jefferson, and J. S. Border, "Subnanosecond GPS-Based Clock Synchronization and Precision Deep-Space Tracking," *TDA Progress Report 42-111,* vol. July–September 1992, http://tmo.jpl.nasa.gov/progress_report/issues.html Accessed October 16, 2000.

[11] L. E. Young et al., "Formation of a GPS-Linked Global Ensemble of Hydrogen Masers and Comparison to JPL's Linear Ion Trap," *Proceedings of the 1996 IEEE International Frequency Control Symposium,* Honolulu, Hawaii, pp. 1159–1162, June 5–7, 1996.

[12] D. C. Jefferson, S. M. Lichten, and L. E. Young, "A Test of Precision GPS Clock Synchronization," *Proceedings of the 1996 IEEE International Frequency Control Symposium,* Honolulu, Hawaii, pp. 1206–1210, June 5–7, 1996.

[13] G. J. Dick, R. T. Wang, and R. L. Tjoelker, "Cryo-Cooled Sapphire Oscillator with Ultra-high Stability," *Proceedings of the 1998 IEEE International Frequency Control Symposium,* Pasadena, California, pp. 528–533, May 27–29, 1998.

[14] R. L. Tjoelker, J. D. Prestage, and L. Maleki, "Record Frequency Stability with Mercury in a Linear Ion Trap," *Proceedings of the Fifth Symposium on Frequency Standards and Metrology,* Woods Hole, Massachusetts, pp. 33–38, October 15–19, 1995.

[15] G. J. Dick and R. T. Wang, "Cryo-Cooled Sapphire Oscillator for the Cassini Ka-band Experiment," *Proceedings of the 1997 IEEE International Frequency Control Symposium,* Orlando, Florida, pp. 1009–1014, May 28–30, 1997.

[16] *Deep Space Network/Flight Project Interface Design Handbook, Vol. 1: Existing DSN Capabilities,* JPL 810-5, Module TRK-30, Rev. E, http://eis.jpl.nasa.gov/deepspace/dsndocs/810-005/ Accessed November 6, 2000.

[17] R. Woo and J. W. Armstrong, "Spacecraft Radio Scattering Observations of the Power Spectrum of Electron Density Fluctuations in the Solar Wind," *Journal of Geophysical Research,* vol. 84, no. A12, pp. 7288–7296, December 1, 1979.

[18] W. A. Coles and J. K. Harmon, "Propagation Observations of the Solar Wind Near the Sun," *The Astrophysical Journal,* vol. 337, no. 2, pp. 1023–1034, February 1989.

[19] P. F. MacDoran, "A First-Principles Derivation of the Differenced Range Versus Integrated Doppler (DRVID) Charged Particle Calibration Method," *Space Programs Summary 37-62, Vol. II, The Deep Space Network,* Jet Propulsion Laboratory, Pasadena, California, pp. 28–34, March 1970.

[20] D. W. Green, V. W. Lam, and H. N. Royden, "Effects of the Charged Particle Environment on Voyager Navigation at Jupiter and Saturn," AIAA 80-1650 paper presented at the AIAA/AAS Astrodynamics Conference, Danvers, Massachusetts, August 11–13, 1980.

[21] C. M. Ho, B. D. Wilson, A. J. Mannucci, U. J. Lindqwister, and D. N. Yuan, "A Comparative Study of Ionospheric Total Electron Content Measurements and Models with TOPEX," *Radio Science,* vol. 32, no. 4, pp. 1499–1512, July–August 1997.

[22] G. E. Lanyi, "Tropospheric Delay Effects in Radio Interferometry," *TDA Progress Report 42-78,* vol. April–June 1984, http://tmo.jpl.nasa.gov/progress_report/issues.html Accessed October 16, 2000.

[23] A. Niell, "Global Mapping Functions for the Atmospheric Delay at Radio Wavelengths," *Journal of Geophysical Research,* vol. 101, no. B2, pp. 3227–3246, February 10, 1996.

[24] V. de Brito Mendes, "Modeling the Neutral-Atmosphere Propagation Delay in Radiometric Space Techniques," University of New Brunswick [Canada] Technical Report 199, April 1999.

[25] G. Elgered, "Tropospheric Radio Path Delay From Ground-Based Microwave Radiometry," *Atmospheric Remote Sensing by Microwave Radiometry* (M. Janssen, editor), New York: Wiley & Sons, 1992.

[26] R. N. Treuhaft and G. E. Lanyi, "The Effect of the Dynamic Wet Troposphere on Radio Interferometric Measurements," *Radio Science,* vol. 22, no. 2, pp. 251–265, March–April 1987.

[27] S. M. Lichten, "Precise Estimation of Tropospheric Path Delays with GPS Techniques," *TDA Progress Report 42-100,* vol. October–December 1989, http://tmo.jpl.nasa.gov/progress_report/issues.html Accessed October 16, 2000.

[28] A. B. Tanner, "Development of a High-Stability Water Vapor Radiometer," *Radio Science,* vol. 33, no. 2, pp. 449–462, March–April 1998.

[29] R. Beer, *Remote Sensing by Fourier Transform Spectrometry,* New York: John Wiley & Sons, 1992.

[30] G. M. Resch et al., "Calibration of Atmospherically Induced Delay Fluctuations Due to Water Vapor," NASA/CP-2000-209893, *International VLBI Service for Geodesy and Astrometry, 2000 General Meeting Proceedings* (N. R. Vandenberg and K. D. Baver, editors), Kötzting, Germany, pp. 274–279, February 21–24, 2000.

[31] O. J. Sovers and C. S. Jacobs, *Observation Model and Parameter Partials for the JPL VLBI Parameter Estimation Software MODEST—1996,* JPL Publication 83-39, Rev. 6, Jet Propulsion Laboratory, Pasadena, California, August 1996.

[32] J. A. Steppe, S. H. Oliveau, and O. J. Sovers, "Earth Rotation Parameters from DSN VLBI: 1995," in *Earth Orientation, Reference Frames and Atmospheric Excitation Functions Submitted for the 1994 IERS Annual Report: IERS Technical Note 19* (P. Charlot, editor), pp. R21–R27, Paris: Observatoire de Paris, September 1995.

[33] C. S. Jacobs et al., "The JPL Extragalactic Radio Reference Frame: Astrometric Results of 1978–96 Deep Space Network VLBI," *TMO Progress Report 42-133,* vol. January–March 1998, http://tmo.jpl.nasa.gov/progress_report/issues.html Accessed October 16, 2000.

[34] C. Boucher, Z. Altamimi, and P. Sillard, *The 1997 International Terrestrial Reference Frame (ITRF97): IERS Technical Note 27,* Paris: Observatoire de Paris, May 1999.

[35] C. Boucher, Z. Altamimi and L. Duhem, *Results and Analysis of the ITRF93: IERS Technical Note 18,* Paris: Observatoire de Paris, October 1994.

[36] W. M. Folkner, "DSN Station Locations and Uncertainties," *TDA Progress Report 42-128,* vol. October–December 1996, http://tmo.jpl.nasa.gov/progress_report/issues.html Accessed October 16, 2000.

[37] K. Lambeck, *The Earth's Variable Rotation,* New York: Cambridge University Press, 1980.

[38] T. M. Eubanks et al., "Causes of Rapid Motions of the Earth's Pole," *Nature,* vol. 334, no. 6178, pp. 115–119, July 14, 1988.

[39] R. Hide, "Rotation of the Atmospheres of the Earth and Planets," *Philosophical Transactions of the Royal Society, Series A,* vol. 313, no. 1524, pp. 107–121, November 27, 1985.

[40] J. M. Wahr, "The Effects of the Atmosphere and Oceans on the Earth's Wobble; I, Theory," *Geophysical Journal of the Royal Astronomical Society,* vol. 70, no. 2, pp. 349–372, 1982.

[41] R. S. Gross, "The Excitation of the Chandler Wobble," *Geophysical Research Letters,* vol. 27, no. 15, pp. 2329–2332, August 1, 2000.

[42] J. M. Wahr, "Geophysical Aspects of Polar Motion, Variations in Length of Day, and the Luni-solar Nutations," chapter in *Space Geodesy and Geodynamics* (A. J. Anderson and A. Cazenave, editors), London: Academic Press, 1986.

[43] K. Lambeck, "Geophysical Geodesy," chapter in *The Slow Deformation of the Earth,* Oxford: Clarendon Press, 1988.

[44] R. Hide and J. O Dickey, "Earth's Variable Rotation," *Science,* vol. 253, no. 5020, pp. 629–637, August 9, 1991.

[45] A. P. Freedman et al., "The Short-term Prediction of Universal Time and Length of Day Using Atmospheric Angular Momentum," *Journal of Geophysical Research,* vol. 99, no. B4, pp. 6981–6996, April 1994.

[46] *Support Instrumentation Requirements Document for the 1989 Galileo Project,* Galileo Project Document 625-501, Rev. A, JPL D-476, Rev. A (internal document), Jet Propulsion Laboratory, Pasadena, California, May 1, 1988.

[47] *Mars Pathfinder Project Policies and Requirements Document,* JPL D-10856, Rev. C (internal document), Jet Propulsion Laboratory, Pasadena, California, January 1995.

[48] D. D. Morabito, T. M. Eubanks, and J. A. Steppe, "Kalman Filtering of Earth Orientation Changes," chapter in *The Earth's Rotation and Refer-*

ence Frames for Geodesy and Geodynamics (A. K. Babock and G. A. Wilkins, editors), pp. 257–267, IAU, 1988.

[49] R. S. Gross et al., "A Kalman-Filter-Based Approach to Combining Independent Earth-Orientation Series," *Journal of Geodesy,* vol. 72, no. 4, pp. 215–235, April 1998.

[50] R. S. Gross, "Combinations of Earth Orientation Measurements: SPACE97, COMB97, and POLE97," *Journal of Geodesy,* vol. 73, no. 12, pp. 627–637, February 2000.

[51] R. S. Gross, *Combinations of Earth Orientation Measurements: SPACE98, COMB98, and POLE98,* JPL Publication 99-6, Jet Propulsion Laboratory, Pasadena, California, April 1999.

[52] R. S. Gross, *Combinations of Earth Orientation Measurements: SPACE99, COMB99, and POLE99,* JPL Publication 00-5, Jet Propulsion Laboratory, Pasadena, California, April 2000.

[53] T. A. Herring, C. R. Gwinn, and I. I. Shapiro, "Geodesy by Radio Interferometry: Studies of the Forced Nutations of the Earth, Part 1: Data Analysis," *Journal of Geophysical Research,* vol. 91, no. B5, pp. 4745–4754, April 10, 1986.

[54] C. Ma et al., "The International Celestial Reference Frame as Realized by Very Long Baseline Interferometry," *The Astronomical Journal,* vol. 116, no. 1, pp. 516–546, July 1998.

[55] J. A. Estefan and W. M. Folkner, "Sensitivity of Planetary Cruise Navigation to Earth Orientation Calibration Errors," *TDA Progress Report 42-123,* vol. July–September 1995, http://tmo.jpl.nasa.gov/progress_report/issues.html Accessed October 16, 2000.

[56] J. J. Spilker, Jr., "GPS Signal Structure and Performance Characteristics," *Global Positioning System,* ION 0-936406-00-3, pp. 29–54, 1980.

[57] B. W. Parkinson and J. J. Spilker, Jr., editors, *Global Positioning System: Theory and Applications, Volume I,* Progress in Astronautics and Aeronautics, vol. 163, AIAA, 1996.

[58] B. W. Parkinson and J. J. Spilker, Jr., editors, *Global Positioning System: Theory and Applications, Volume II,* Progress in Astronautics and Aeronautics, vol. 164, AIAA, 1996.

[59] S. M. Lichten, "Estimation and Filtering for High-Precision GPS Applications," *Manuscripta Geodaetica,* vol. 15, pp. 159–176, 1990.

[60] International GPS Service, http://igscb.jpl.nasa.gov/igscb/station/general/rcvr_ant.tab Accessed September, 12, 2000.

[61] J. F. Zumberge and W. I. Bertiger, "Ephemeris and Clock Navigation Message Accuracy," chapter in *Global Positioning System: Theory and*

Applications, Volume I (B. W. Parkinson and J. J. Spilker, Jr., senior editors), Progress in Astronautics and Aeronautics, AIAA, 1996.

[62] R. R. Hatch, R. Keegan, and T. A. Stansell, "Kinematic Receiver Technology for Magnavox," *Sixth International Geodetic Symposium on Satellite Positioning,* Columbus, Ohio, pp. 174–183, March 17–20, 1992.

[63] T. K. Meehan et al, "The TurboRogue Receiver," *Sixth International Geodetic Symposium on Satellite Positioning,* Columbus, Ohio, pp. 209–218, March 17–20, 1992.

[64] J. B. Thomas, *Signal Processing Theory for the TurboRogue Receiver,* JPL Publication 95-6, Jet Propulsion Laboratory, Pasadena, California, April 1, 1995.

[65] C. L. Thornton, S. M. Lichten, L. E. Young, and T. P. Yunck, "Novel Concepts for Precise Low Earth Orbiter Navigation with GPS," IAF-97-M.6-01, 48th International Astronautical Congress, Turin, Italy, October 6–10, 1997.

[66] G. Blewitt et al., "Global Coordinates with Centimeter Accuracy in the International Terrestrial Reference Frame Using GPS," *Geophysical Research Letters,* vol. 19, no. 9, pp. 853–856, May 4, 1992.

[67] W. I. Bertiger et al., "GPS Precise Tracking of TOPEX/Poseidon: Results and Implications," *Journal of Geophysical Research: Oceans,* vol. 99, no. C12, pp. 24449–24464, December 15, 1994.

[68] J. Ceva, "Hughes Aircraft's Architectural Design of the Federal Aviation Administration Wide Area Augmentation System: An International System," IAF-97-M6.04, 48th International Astronautical Congress, Turin Italy, October 6–10, 1997.

[69] W. I. Bertiger et al., "A Real-time Wide Area Differential GPS System," *Journal of Navigation,* vol. 44, no. 4, pp. 433–447, Winter 1997.

[70] R. J. Muellerschoen, W. I. Bertiger, M. F. Lough, D. Stowers, and D. Dong, "An Internet-Based Global Differential GPS System, Initial Results," Institute of Navigation, *2000 National Technical Meeting,* Anaheim, California, pp. 220–225, January 26–28, 2000.

[71] R. J. Muellerschoen, W. I. Bertiger, and M. F. Lough, "Results of an Internet-Based Dual-Frequency Global Differential GPS System," *IAIN World Congress in Association with the U.S. ION 56th Annual Meeting,* San Diego, California, pp. 796–802, June 26–28, 2000.

[72] *International GPS Service for Geodynamics 1998 Annual Report,* JPL 400-839, Jet Propulsion Laboratory, Pasadena, California, July 1999.

[73] R. E. Neilan, J. F. Zumberge, G. Beutler, and J. Kouba, "The International GPS Service: A Global Resource for GPS Applications and Research,"

ION-GPS-97, Kansas City, Missouri, pp. 883–889, September 16–19, 1997.

[74] U. J. Lindqwister, S. M. Lichten, and E. S. Davis, "The GPS TOPEX/Poseidon Precise Orbit Determination Experiment: Implications for Design of GPS Global Networks," IAF-93-A.5.38, 44th Congress of the International Astronautical Federation, Graz, Austria, October 16–22, 1993.

[75] F. H. Webb and J. F. Zumberge, editors, *An Introduction to Gipsy/Oasis II,* JPL D-11088 (internal document), Jet Propulsion Laboratory, Pasadena, California, July 1993.

[76] *1998 IERS Annual Report,* Paris: Observatoire de Paris, 1999.

[77] R. J. Muellerschoen, S. M. Lichten, U. J. Lindqwister, and W. I. Bertiger, "Results of an Automated GPS Tracking System in Support of TOPEX/Poseidon and GPSMet," *ION GPS-95,* Palm Springs, California, pp. 183–193, September 12–15, 1995.

[78] Y. E. Bar-Sever, P. M. Kroger, and J. A. Borjesson, "Estimating Horizontal Gradients of Tropospheric Path Delay with a Single GPS Receiver," *Journal of Geophysical Research,* vol. 103, no. B3, pp. 5019–5035, March 10, 1998.

[79] G. Petit et al., "Use of GPS Ashtech Z12T Receivers for Accurate Time and Frequency Comparisons," *IEEE Transactions on Ultrasonics, Ferroelectrics and Frequency Control,* vol. 46, no. 4, pp. 941–949, July 1999.

[80] G. E. Lanyi and T. Roth, "A Comparison of Mapped and Measured Total Ionospheric Electron Content Using Global Positioning System and Beacon Satellite Observations," *Radio Science,* vol. 23, no. 4, pp. 483–492, July–August 1988.

[81] B. D. Wilson and A. J. Mannucci, "Extracting Ionospheric Measurements from GPS in the Presence of Anti-Spoofing," *ION GPS-94,* Salt Lake City, Utah, pp.1599–1608, September 20–23, 1994.

[82] A. J. Mannucci et al., "A Global Mapping Technique for GPS-Derived Ionospheric Total Electron Content Measurements," *Radio Science,* vol. 33, no. 3, pp. 565–582, May–June 1998.

[83] B. A. Iijima et al., "Automated Daily Process for Global Ionospheric Total Electron Content Maps and Satellite Ocean Altimeter Ionospheric Calibration Based on Global Positioning System Data," *Journal of Atmospheric and Solar-Terrestrial Physics,* vol. 61, no. 16, pp. 1205–1218, November 1, 1999.

[84] W. Ross Stone, editor, *Review of Radio Science 1996–1999,* IEEE PC5838, August 1999.

[85] A. J. Mannucci et al., "Assessment of Global TEC Mapping Using a Three-Dimensional Electron Density Model," *Journal of Atmospheric and Solar-Terrestrial Physics,* vol. 61, no. 16, pp. 1227–1236, November 1, 1999.

[86] R. D. Reasenberg et al., "Viking Relativity Experiment: Verification of Signal Retardation by Solar Gravity," *The Astrophysical Journal,* vol. 234, no. 3, pp. L219–L221, December 15, 1979.

[87] R. W. Hellings et al., "Experimental Test of the Variability of G Using Viking Lander Ranging Data," *Physical Review Letters,* vol. 51, no. 18, pp. 1609–1612, October 31, 1983.

[88] L. E. Young, "Improved Ranging Systems," *Workshop on Relativistic Gravitation Experiments in Space,* NASA CP 3046, Annapolis, Maryland, pp. 203–205, June 28–30, 1989.

[89] J. F. Jordan and L. J. Wood, "Interplanetary Navigation: An Overview," *The Journal of the Astronautical Sciences,* vol. 32, no. 1, pp. 17–28, January–March 1984.

[90] T. McElrath, "Ulysses Orbit Determination at High Declinations," *Flight Mechanics/Estimation Theory Symposium, 1995,* NASA CP 3299, Goddard Space Flight Center, Greenbelt, Maryland, pp. 227–287, May 16–18, 1995.

[91] D. W. Curkendall, "Radiometric Technology for Deep Space Navigation: A Development Overview," AIAA 78-1395, paper presented at the AIAA/AAS Astrodynamics Conference, Palo Alto, California, August 7–9, 1978.

[92] V. J. Ondrasik and K. H. Rourke, "Application of Quasi-VLBI Tracking Data Types to the Zero Declination and Process Noise Problems," AAS 71-399, paper presented at the AAS/AIAA Astrodynamics Specialist Conference, Fort Lauderdale, Florida, August 17–19, 1971.

[93] T. H. Taylor et al., "Orbit Determination for the Voyager II Uranus Encounter," AIAA 86-2112, *Astrodynamics Conference,* Williamsburg, Virginia, pp. 178–191, August 18–20, 1986.

[94] W. G. Melbourne, "Navigation Between the Planets," *Scientific American,* vol. 234, no. 6, pp. 58–74, June 1976.

[95] T. H. Taylor et al., "Performance of Differenced Range Data Types in Voyager Navigation," *TDA Progress Report 42-71,* vol. July–September 1982, http://tmo.jpl.nasa.gov/progress report/issues.html Accessed October 16, 2000.

[96] C. S. Christensen and S. J. Reinbold, "Navigation of the Mariner 10 Spacecraft to Venus and Mercury," *Journal of Spacecraft and Rockets,* vol. 12, no. 5, pp. 280–286, May 1975.

[97] S. W. Thurman, T. P. McElrath, and W. M. Pollmeier, "Short-Arc Orbit Determination Using Coherent X-Band Ranging Data," AAS 92-109, *Advances in the Astronautical Sciences, Volume 79, Part 1* (R. E. Diehl et al., editors), proceedings of the AAS/AIAA Spaceflight Mechanics Meeting, Colorado Springs, Colorado, pp. 23–44, February 24–26, 1992, San Diego, California: Univelt, 1992.

[98] S. R. Poole, M. P. Ananda, and C. E. Hildebrand, "Radio Interferometric Measurements for Accurate Planetary Orbiter Navigation," *Advances in the Astronautical Sciences, Volume 40, Part 1* (P. Penso et al., editors), proceedings of the AAS/AIAA Astrodynamics Specialist Conference, Provincetown, Massachusetts, pp. 93–111, June 25–27, 1979, San Diego, California: Univelt, 1980.

Chapter 4
VLBI Tracking Observables

4.1 VLBI System Description

This section introduces the concept of VLBI tracking and examines major system elements. VLBI technology makes use of the broadband microwave radiation emitted by extragalactic radio sources such as quasars. The signals are typically very weak (< 1 Jy or 10^{-26} W Hz^{-1} m^{-2} of aperture); hence the need for relatively large antennas, low-noise receivers, and wideband recording devices. The DSN had an operational VLBI system for spacecraft tracking (referred to as the Narrow Channel Bandwidth [NCB] VLBI System [1,2]) from 1984 through 1998. The system operated at S-band and X-band on 34- and 70-m antennas. System temperatures were approximately 20 K at S-band and 30 K at X-band. The system recorded open loop at 500 kbit/s. The record rate of 500 kbit/s was chosen to facilitate near-real-time data transmission and processing for navigation support. This moderate data rate led to the descriptive system title "narrow," in contrast with other radio astronomy systems, which operate at data rates of hundreds of megabits per second. Observables generated by the VLBI system are sometimes referred to as "instantaneous angles," even though several minutes of integration time are typically necessary to reduce the error caused by system noise to a level comparable to other measurement errors.

Consider the situation in Fig. 4-1, where the wavefront from a distant source arrives as a plane wave at two widely separated antennas. The signals are amplified, heterodyned to baseband, digitized, time tagged and recorded. The recorded signals are subsequently cross-correlated to determine the difference in the signal time of arrival at the two stations. This differential arrival time is referred to as the VLBI delay and is composed of a geometric delay plus

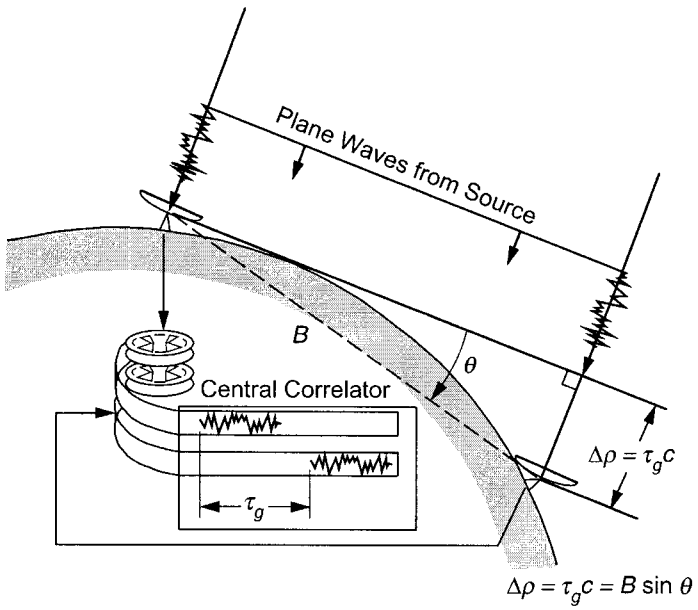

Fig. 4-1. Measuring angles with VLBI. Differential signal arrival time, τ_g, is obtained by cross-correlating signals recorded open loop at each end of the baseline.

delays due to station clock offsets and differences in signal delays through the ionosphere, troposphere, instrumentation, and so forth. The geometric delay can be expressed as

$$\tau_g = \frac{1}{c}\boldsymbol{B} \cdot \hat{s} \tag{4.1-1}$$

where $\boldsymbol{B}$ is the baseline vector between the two stations and $\hat{s}$ is the unit vector in the source direction. Thus, with a priori knowledge of the baseline length and orientation, one can infer from the geometric delay one angular component of the source position. The accuracy to which this angle can be measured depends not only on the precision of the VLBI delay measurement, but also on the accuracy to which the measurement can be calibrated for station clock offsets, differential instrumental and media delays, and baseline orientation errors.

Though the NCB VLBI system has now been retired, a modern system with improved capabilities is being implemented in 2000 and 2001. The new system is based on the Full Spectrum Recorder (FSR), which is used in the DSN for telemetry arraying and for open-loop radio science recordings [3–5], and is referred to as the VLBI Science Receiver (VSR). Data processing will be

done by software, on a workstation. Computer speeds are adequate today so that narrow-bandwidth VLBI data may be correlated in a timely manner, without the need for special-purpose hardware.

4.1.1 Delta VLBI

One means for effectively reducing the contribution of uncalibrated errors in VLBI delay measurements is to introduce a second measurement, that of an angularly nearby source whose position is well known. Explicit differencing of observations from angularly nearby sources removes or substantially reduces the effects of common errors. For example, station clock offsets and instrumental group delays may be almost entirely cancelled. In this way, errors due to uncalibrated media effects and poorly modeled baseline vectors can be greatly reduced. The extent to which such errors are eliminated in the differential observable depends upon the commonality of the signal path, for example, how angularly close the sources are, the time offset between observations, and the degree to which the spectral characteristics of the signals are similar.

If one of the sources is a distant spacecraft and the other is a quasar, the spectral structures of the signals will differ significantly. Natural sources have broadband signals with nearly flat spectra spread over many gigahertz. Spacecraft signals, on the other hand, are band-limited (for example, 40 MHz at X-band), and contain a number of tones that are utilized for VLBI tracking. Open-loop recordings are made for each source, using frequency channels centered at the spacecraft tone frequencies. This is done so that instrumental effects will be as common as possible for the two sources. The recorded data are then transmitted from each station to a common workstation at JPL. At this point, the quasar signal phase is extracted by cross-correlation of the frequency channels between stations. The phase of each spacecraft tone is extracted by local model correlation, a process whereby the signal is mixed with a computer-generated model of the expected signal. Differencing tone phase between stations provides a measurement analogous to the cross-correlation phase for a quasar.

Measurements made from a single frequency channel yield phase delay to a fraction of a cycle. The total delay is ambiguous to λn, where n is an integer number of radio frequency (RF) cycles and λ is the wavelength. Multiple measurements of channels properly spaced in the frequency band enable the determination of unambiguous delay through a process referred to as bandwidth synthesis [6]. In this process, ambiguities are first resolved for the narrowest effective bandwidth, and then successively for wider bandwidths. After cycle ambiguities are resolved, delay is obtained as the slope of the phase versus frequency line. The unambiguous delay obtained from spacecraft measurements is referred to as differential one-way range (DOR), and the tones in the spacecraft spectrum from which the measurement is derived are referred to as DOR

tones. The differential delay between spacecraft and quasar is termed ΔDOR, and yields a highly accurate measure of the spacecraft angular position in the radio source reference frame.

Ambiguous measurements of phase delays yield information only on the delay rate. This measurement type is important, however, since it may be obtained from spacecraft that emit only a carrier signal. Several hours of phase-delay-rate data may be used to infer angular coordinates in much the same way as Doppler measurements [7]. For a planetary orbiter, phase-delay-rate data directly measure the orientation of the orbit plane about the line of sight from Earth to the planet, as noted in Section 3.6.

4.1.2 Radio Source Reference Frame

One of the key characteristics of VLBI tracking technology is the development over the last two decades of a highly stable and accurate quasi-inertial reference frame with the associated catalog of approximately 200 source positions [8,9]. Source positions are determined in the ICRF with an internal consistency of better than 5 nrad [10]. This reference frame was adopted by the IAU in 1998 as the fundamental celestial reference frame, replacing the optical reference frame known as FK5. Among the by-products of the source catalog development are estimates of DSN baselines and improved models for precession and nutation [8,9,11]. Measured baseline lengths are consistent with plate tectonic models to about the 2-cm level. As noted in Section 3.3.4.1, Earth-fixed coordinates for most DSN stations have been determined to 3 cm or better in all components, using a combination of VLBI and other space geodetic techniques [12]. The newer sites have not yet been surveyed to this level.

A separate receiving system, which operates at a higher data rate than the NCB system, is used in the DSN to support the source catalog development effort. Data were acquired from 1978 to 1989 using the Mark II VLBI system [13], and since then using the Mark III VLBI system [14]. The installation of Mark III terminals operating at 112 Mbit/s, coupled with low-noise amplifiers having 400-MHz bandwidth and other improvements, have greatly increased the sensitivity of the system. These improvements continue to enable further advances in source position and baseline accuracies.

4.1.3 Radio and Planetary Frame Tie

Navigation to the planets using VLBI tracking requires knowledge of planetary ephemerides in the radio reference frame. The planetary ephemerides have evolved from many decades of observations, largely Earth-based optical and radar, supplemented with planetary encounter data and laser ranging to the moon [15]. Analyses of these data have produced lunar and planetary ephemerides in a self-consistent reference frame tied to the dynamical equinox and precessed to the epoch J2000 [16]. The most recent ephemerides are also fit to

frame-tie data that directly align the planetary ephemeris with the ICRF [17,18]. The internal precision of the planetary ephemeris reference frame rivals that of the ICRF, at the 5-nrad level [19], but most individual bodies are not known to this level.

Within the planetary ephemeris frame, the positions of Venus, Mars, Earth, and the moon are all known to the 5-nrad level, due primarily to accurate measurements made over the last 30 years. Sources of these measurements include LLR, precise radio ranging to the Viking and Pathfinder landers, radar ranging to Venus, and ΔDOR measurements of the Magellan orbiter at Venus. The position of Mercury is known only to the 25-nrad level. Of the outer planets, Jupiter's position is best known at the 100-nrad level, due to ranging to the Voyager and Ulysses spacecraft, and ΔDOR measurements of the Ulysses and Galileo spacecraft [20,21]. The positions of the other large outer planets are known only to about the 250-nrad level, while the position of Pluto is uncertain at the microradian level [22,23].

The remaining uncertainty in the orientation of the planetary ephemeris frame with respect to the radio frame is at the 5-nrad level in all components [17]. This accuracy has only recently been achieved. The offset in the origin of right ascension was hundreds of nanoradians until the first VLBI measurements were made of spacecraft at planetary encounters. The Mars Viking and the Pioneer Venus orbiters provided an early opportunity for measuring the planetary-radio frame offset. The position of each orbiter relative to the planet was determined from Earth-based Doppler tracking. Delta VLBI phase-delay-rate measurements between the orbiter and an angularly nearby radio source then provided a measure of the frame tie. Accuracies of about 100 nrad in both right ascension and declination were achieved [24]. Experiments to refine the frame tie included measurements of millisecond pulsars and the timing of occultations of radio sources by planetary objects. But the first significant improvement in knowledge of the frame tie was made in the early 1990s by comparing the terrestrial reference frames associated with VLBI and LLR data analyses. The VLBI solutions tie the DSN stations to the radio frame, while the LLR solutions are closely tied to the planetary ephemeris reference frame [16]. The tie between the DSN and the LLR stations is determined from common site measurements made by the NASA Crustal Dynamics Project, using VLBI and SLR. The frame tie was determined by this method to 15 nrad in each component [25]. This accuracy was confirmed and improved to the 5-nrad level by the acquisition of 18 ΔDOR measurements of the Magellan orbiter at Venus between 1990 and 1994 [17,26].

4.1.4 VLBI Calibration System

While the ΔVLBI system is largely self-calibrating, a number of errors do not totally cancel when measurements to individual sources are differenced.

For example, the cancellation of errors due to PM, UT, station locations, and media delays is dependent upon the angular distance between sources. In order to minimize these effects in the tracking observable, it is necessary to select radio sources angularly close to the spacecraft and apply the most accurate available calibrations for these effects. Previously, the NCB VLBI system itself provided the DSN with accurate means for timely determination of UT, PM, and clock parameters. The GPS calibration system, anchored by monthly wide-band VLBI measurements, is now used for this purpose. The GPS calibration system is also used to generate line-of-sight calibrations for ionospheric delays and calibrations for zenith tropospheric delays (see Chapter 3).

4.1.5 Major Error Sources

The major sources of error in present day ΔVLBI observations are typically measurement signal-to-noise ratios (SNRs), uncalibrated troposphere delays, baseline errors, and instrumental delays (see Fig. 4-2). Models for estimating these measurement errors have been developed [27]. This section summarizes the major system design and calibration limitations to overall performance. Expectations for future system improvements are presented in Chapter 5.

The magnitude of each error source in VLBI is highly dependent upon system operating parameters. For example, SNR for quasar measurements depends upon quasar flux density, recording bandwidth, system temperature, antenna diameter and efficiency, and integration time. Although trade-offs may be made between such variables as antenna size, source strength, and integration time, they may be constrained by other considerations, such as the availability of sufficiently strong sources angularly close to the spacecraft. Ideally, one would like to find strong (1-Jy) sources within a few degrees of the spacecraft, but this situation is more the exception than the rule.

Consider the map of available sources for VLBI tracking of the Galileo spacecraft, shown in Fig. 4-3. Catalog sources within a 15-deg band about the Galileo trajectory vary in strength from 1 Jy down to 0.1 Jy. It should be noted that the scarcity of known sources near the encounter coordinates is due to the intersection of the ecliptic and galactic planes. The direction specified by 18-h right ascension and –23-deg declination is in the plane of the Milky Way, directly toward the galactic center. The large quantity of radio emissions originating within our own galaxy has hampered efforts to survey and catalog compact extragalactic radio sources in this direction. For ΔDOR measurements, a source strength of 0.4 Jy was required using a 70-m and 34-m DSN antenna pair with the now-retired NCB VLBI system and a 10-min integration time. The new VSR design has the capability to support a higher data recording rate that will lower the source detection threshold by a factor of two or more. This increased sensitivity will allow the selection of a weaker source angularly closer to the spacecraft, or the use of smaller antennas.

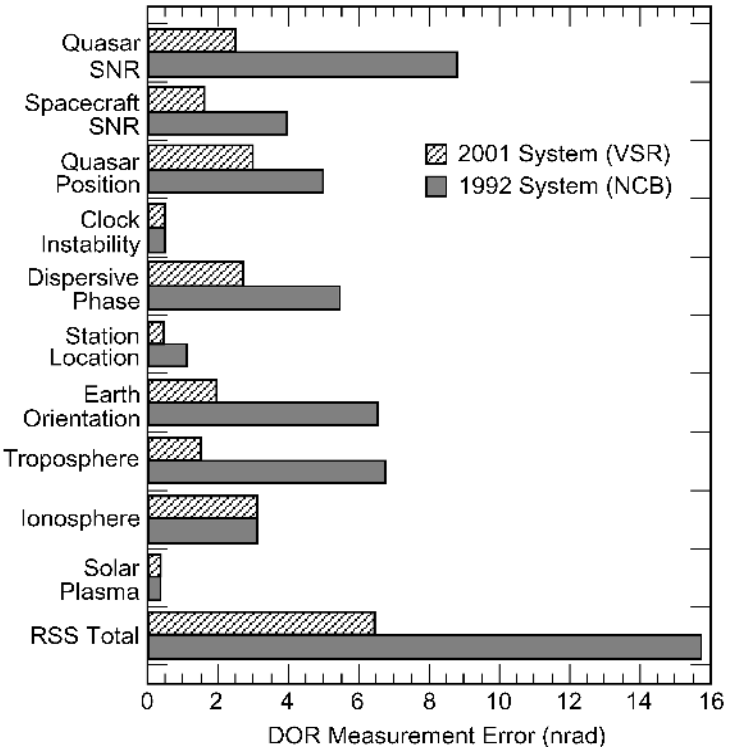

Fig. 4-2. Error budget for spacecraft-quasar ΔDOR delay measurements for both the prior- and next-generation tracking systems, consistent with system characteristics given in Table 4-1.

While most errors scale down with angular separation between the spacecraft and the quasar, instrumental errors depend more on the characteristics of the radio signals. In particular, dispersive instrumental effects in ΔDOR measurements are inversely proportional to the total spanned bandwidth of the recorded signals. Limitations on spanned bandwidth are typically imposed by the spacecraft radio design; the quasars are sufficiently broadband. Moreover, the DSN front end can accommodate 400 MHz at X-band and 100 MHz at S-band. On the other hand, for all spacecraft currently in flight at the time of publication, the widest DOR tone spacing is 38 MHz at X-band. International frequency allocations limit spacecraft transmissions to 50 MHz at X-band. However, the allocated bandwidth at Ka-band is 500 MHz [28]. Future ΔDOR systems, operating at Ka-band and utilizing tones separated by 200 MHz, will greatly reduce instrumental and other dispersive errors.

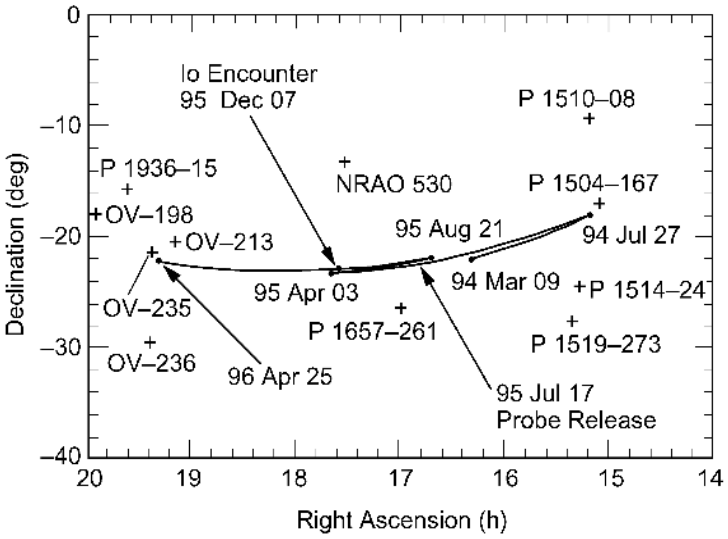

Fig. 4-3. Angular components of Galileo spacecraft trajectory during the Jupiter approach. Also shown are catalog radio sources within 15 deg of the trajectory and having flux greater than 0.1 Jy.

4.2 Spacecraft VLBI System Performance

Interferometric measurements directly determine angular components of spacecraft state. The inclusion of ΔDOR data with long arcs of Doppler and range data desensitizes trajectory solutions to mismodeled dynamic forces, and can improve knowledge of spacecraft position by a factor of five or more. The realized improvement in trajectory accuracy with respect to a target depends on knowledge of the target position in the radio frame. Both the Galileo and Mars Observer projects had a requirement for ΔDOR measurements with a one-sigma accuracy of 50 nrad during their interplanetary cruise phases. Requirements to deliver landers to the surface of Mars are expected to be in the range of 5 to 10 nrad.

The contribution of individual error sources to the overall measurement accuracy is known as the error budget. An error budget for ΔDOR measurements is shown in Fig. 4-2. The estimate labeled "1992" assumes a spacecraft DOR tone spacing of 38 MHz at X-band along with use of the NCB system, and hence applies to both Galileo and Mars Observer. The performance of the NCB VLBI system on Galileo and Mars Observer was balanced in that errors due to thermal noise, station instrumentation, platform parameters, and media delays

were comparable in size. Measurement errors were estimated using the formulations in [27]. See Table 3-3 for assumptions on calibration system accuracies. See Table 4-1 for assumptions on receiving system characteristics and observation geometry. As shown in Fig. 4-2, the typical accuracy of the ΔDOR system in 1992 was 16 nrad. However, some items in the error budget depend strongly on geometry. With other assumptions fixed as in Tables 3-3 and 4-1, measurement accuracy of 50 nrad was possible for even the most unfavorable geometries involving spacecraft in the ecliptic observed from DSN baselines. In the final analysis, the performance of the NCB system was adequate to meet navigation requirements of the Galileo and Mars Observer missions.

Interferometric measurements have also been made of several spacecraft not equipped with DOR tones. Differential one-way range measurements were acquired by using harmonics of a spacecraft telemetry subcarrier signal. This technique was employed to enhance cruise navigation for the Voyager [29], Magellan [30], and Ulysses [20] spacecraft. However, for these spacecraft, the widest spacing of detectable telemetry signals was somewhat less than the 38 MHz provided by the DOR tones of Galileo and Mars Observer. Specifi-

Table 4-1. Spacecraft-to-quasar ΔDOR assumed characteristics.

Characteristics	Assumed Value	
Spacecraft observing time	10 min	
Spacecraft-to-quasar angular separation	10 deg	
Minimum elevation angle	15 deg	
Elevation angle difference	5 deg	
Quasar flux	0.4 Jy	
Observing band	X-band	
Spanned bandwidth	38.25 MHz	
System noise temperature	30 K	
	VLBI 1992	VLBI 2001
Quasar coordinates	5 nrad	3 nrad
Quasar observing time	10 min	20 min
Radio and planetary frame tie	25 nrad	5 nrad
DSN antennas	70m and 34m	34m and 34m
Channel bandwidth	0.25 MHz	1 MHz
Channel recording	multiplexed	parallel
Phase dispersion	1 deg	0.5 deg

cally, the maximum usable tone spacings for Voyager, Magellan, and Ulysses at X-band were, respectively, 14 MHz, 31 MHz, and 6 MHz. Since system noise and phase-dispersion errors scaled inversely with maximum tone spacing, these components of the error budget were increased by a corresponding amount from the 1992 level shown in Fig. 4-2.

Figure 4-4 displays Magellan ΔDOR residuals acquired early in cruise. The residuals are shown for two trajectories. The white symbols represent the ΔDOR pass-through residuals relative to a trajectory determined from Doppler data spanning the time interval shown in the figure. The black symbols are the ΔDOR residuals to a trajectory fit to both the Doppler and the ΔDOR data (weighted at 50 nrad). Note that the Goldstone-to-Madrid baseline is oriented nearly east-west, so that measurements on this baseline are sensitive to spacecraft right ascension, whereas measurements on the canted Goldstone-to-Canberra baseline are equally sensitive to right ascension and declination. Comparison of the ΔDOR residuals for the Goldstone-to-Madrid baseline from the two solutions shows that the Doppler-only solution does a good job of determining right ascension, although a small drift over the 17-d data arc is apparent. Since right ascension has been determined fairly well, large ΔDOR residuals for the Goldstone-to-Canberra baseline must be attributed to a trajectory error in the declination component. Comparison of these residuals for the two solutions shows that the spacecraft declination determined from Doppler alone is biased by at least 2.3 μrad and drifts by 1.6 μrad over the 17-d data arc. When the ΔDOR data are fit, residuals for both baselines are reduced to the

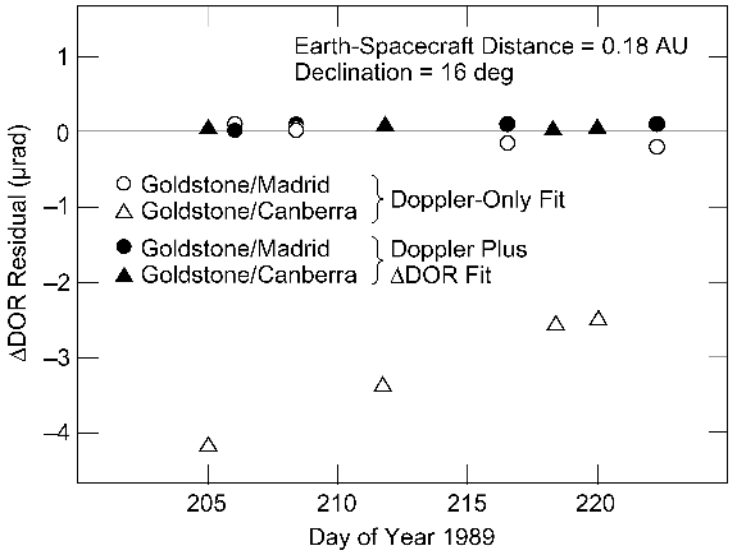

Fig. 4-4. Magellan ΔDOR residuals for two estimated trajectory solutions.

level of the data accuracy, which is 50 nrad. For this case, an improvement of a factor of 46 in solution accuracy was achieved.

The inaccuracy of the Doppler-only solution was due primarily to mismodeled solar pressure accelerations. The effect of the mismodeling was to move the spacecraft position estimate in the direction least well determined by Doppler; that is declination. The ΔDOR data exposed the modeling problem. Further, these data directly measured each angular component, and hence produced an accurate solution even in the presence of mismodeled accelerations. The two solutions illustrated in Fig. 4-4 were interim solutions developed for the purpose of data evaluation.

A similar modeling problem with small forces contributed to the loss of the Mars Climate Orbiter in 1999. A trajectory error accumulated in the declination direction, resulting in inconsistencies in solutions obtained from different data processing strategies. These inconsistencies were not resolved to identify the actual error. Unfortunately, no angular data types were employed as a check against this type of problem. Several reviews were conducted afterwards. In the *Report on Project Management in NASA,* by the Mars Climate Orbiter Mishap Investigation Board [31], one of the "lessons learned" in the section on systems engineering states:

> Develop and deploy alternative navigational schemes to single-vehicle, Deep Space Network tracking for future planetary missions. For example, utilizing "relative navigation" when in the vicinity of another planet is promising.

The planned implementation of a robust, next-generation ΔDOR capability addresses this point.

4.3 Utility of Open-Loop Recordings

Open-loop recordings of radio sources, as is done in VLBI, can be made even if one does not have good a priori knowledge of source position or signal frequency. With open-loop recordings, in the event that the signal is weaker than expected, less stable, or off in frequency, extra effort can be applied during signal processing to generate observables. By contrast, systems that rely on real-time signal detection may fail under these conditions.

Open-loop recordings were used in a scientific investigation during the entry of the Galileo probe into the Jovian atmosphere. The prime radio link during descent was a transmission from the probe to the Galileo orbiter that was flying overhead. The orbiter used a closed-loop radio system to track the probe signal in real time. These Doppler measurements provided a one-dimensional profile of the atmospheric winds. At the same time, open-loop recordings were made of the probe signal at two radio telescope observatories on Earth. Even though the signal received on Earth was a billion times weaker than the prime radio link due to the propagation direction being off the probe antenna boresite

and the significantly larger distance to the probe, the signal was successfully detected in nonreal time and provided a valuable second profile of wind velocity in the Jovian atmosphere [32].

Open-loop recordings and subsequent specialized signal processing were used in 1999 to verify approach navigation for the Mars Polar Lander (MPL) [33,34] and to search for the signal that might have been transmitted by MPL from the surface of Mars [35]. Another use of open-loop techniques (under special circumstances) could be in situ tracking between orbiters at Mars. Analyses of these open-loop recordings, after transmission to Earth, could, if necessary, provide additional information beyond that of onboard closed-loop systems.

References

[1] K. M. Liewer, "DSN Very Long Baseline Interferometry System Mark IV-88," *TDA Progress Report 42-93,* vol. January–March 1988, http://tmo.jpl.nasa.gov/progress_report/issues.html Accessed October 16, 2000.

[2] T. K. Peng et al., "Deep Space Network Enhancement for the Galileo Mission to Jupiter," *Acta Astronautica,* vol. 17, no. 3, pp. 321–330, March 1988.

[3] T. T. Pham et al., "Tracking the Galileo Spacecraft With the DSCC Galileo Telemetry Prototype," *TDA Progress Report 42-119,* vol. July–September 1994, http://tmo.jpl.nasa.gov/progress_report/issues.html Accessed October 16, 2000.

[4] G. E. Wood et al., "Mars Pathfinder Entry, Descent, and Landing Communications," *TDA Progress Report 42-131,* vol. July–September, 1997, http://tmo.jpl.nasa.gov/progress_report/issues.html Accessed October 16, 2000.

[5] T. T. Pham, A. P. Jongeling, and D. H. Rogstad, "Enhancing Telemetry and Navigation Performance with Full Spectrum Arraying," *2000 IEEE Aerospace Conference Proceedings,* Big Sky, Montana, pp. 491–498, March 18–25, 2000.

[6] A. E. E. Rogers, "Very-Long-Baseline Interferometry with Large Effective Bandwidth for Phase-Delay Measurements," *Radio Science,* vol. 5, no. 10, pp.1239–1247, October 1970.

[7] W. G. Melbourne and D. W. Curkendall, "Radio Metric Direction Finding: A New Approach to Deep Space Navigation," paper presented at the AAS/

AIAA Astrodynamics Specialist Conference, Jackson Hole, Wyoming, September 7–9, 1977.

[8] C. S. Jacobs et al., "The JPL Extragalactic Radio Reference Frame: Astrometric Results of 1978–96 Deep Space Network VLBI," *TMO Progress Report 42-133,* vol. January–March 1998, http://tmo.jpl.nasa.gov/progress_report/issues.html Accessed October 16, 2000.

[9] O. J. Sovers, "JPL 1990–3: A 5-nrad Extragalactic Source Catalog Based on Combined Radio Interferometric Observations," *TDA Progress Report 42-106,* vol. April–June 1991, http://tmo.jpl.nasa.gov/progress_report/issues.html Accessed October 16, 2000.

[10] C. Ma et al., "The International Celestial Reference Frame as Realized by Very Long Baseline Interferometry," *The Astronomical Journal,* vol. 116, no. 1, pp. 516–546, July 1998.

[11] J. A. Steppe, S. H. Oliveau, and O. J. Sovers, "Earth Rotation Parameters from DSN VLBI: 1994," in *Earth Orientation, Reference Frames and Atmospheric Excitation Functions Submitted for the 1993 IERS Annual Report: IERS Technical Note 17,* pp. R19–R32, Paris: Observatoire de Paris, September 1994.

[12] W. M. Folkner, "DSN Station Locations and Uncertainties," *TDA Progress Report 42-128,* vol. October–December 1996, http://tmo.jpl.nasa.gov/progress_report/issues.html Accessed October 16, 2000.

[13] B. G. Clark, "The NRAO Tape-Recorder Interferometer System," *Proceedings of the IEEE,* vol. 61, no. 9, pp. 1242–1248, September 1973.

[14] A. E. E. Rogers et al., "Very-Long-Baseline Interferometry: The Mark III System for Geodesy, Astrometry, and Aperture Synthesis," *Science*, vol. 219, no. 4580, pp. 51–54, January 7, 1983.

[15] E. M. Standish, "Celestial Reference Frames: Definitions and Accuracies," chapter in *The Impact of VLBI on Astrophysics and Geophysics* (M. J. Reid and J. M. Moran, editors), proceedings of the 129th IAU Symposium, Cambridge, Massachusetts, May 10–15, 1987, Dordrecht, The Netherlands: D. Reidel, 1988.

[16] J. G. Williams and E. M. Standish, "Dynamical Reference Frames in the Planetary and Earth-Moon Systems," chapter in *Reference Frames in Astronomy and Geophysics* (J. Kovalevsky et al., editors), Dordrecht, The Netherlands: Kluwer, 1989.

[17] E. M. Standish, "JPL Planetary and Lunar Ephemerides, DE405/LE405," JPL Interoffice Memorandum 312.F-98-048 (internal document), Jet Propulsion Laboratory, Pasadena, California, August 26, 1998.

[18] E. M. Standish, "JPL Planetary and Lunar Ephemerides, DE403/LE403," JPL Interoffice Memorandum 314.10-127 (internal document), Jet Propulsion Laboratory, Pasadena, California, May 22, 1995.

[19] C. S. Jacobs et al., "The Extragalactic and Solar System Celestial Frames: Accuracy, Stability, and Interconnection," *Advances in Space Research,* vol. 13, no. 11, pp. (11)161–(11)174, 1993.

[20] W. M. Folkner, T. P. McElrath, and A. J. Mannucci, "Determination of Position of Jupiter from Very-Long Baseline Interferometry Observations of Ulysses," *The Astronomical Journal,* vol. 112, no. 3, pp.1294–1297, September 1996.

[21] R. A. Jacobson et al., "A Comprehensive Orbit Reconstruction for the Galileo Prime Mission in the J2000 System," AAS 99-330, *Advances in the Astronautical Sciences, Volume 103, Part I,* (K. C. Howell, F. R. Hoots, B. Kaufman, K. T. Alfriend, editors), proceedings of the AAS/AIAA Astrodynamics Specialist Conference, Girdwood, Alaska, pp. 465–486, August 16–19, 1999, San Diego, California: Univelt, 1999.

[22] E. M. Standish, "An Approximation to the Outer Planet Ephemeris Errors in JPL's DE-200," *Astronomy and Astrophysics,* vol. 233, no. 1, pp. 272–274, July 1990.

[23] E. M. Standish and J. G. Williams, "Dynamical Reference Frames in the Planetary and Earth-Moon Systems," *Inertial Coordinate Systems on the Sky,* proceedings of the 141st IAU Symposium (J. H. Lieske and V. K. Abalakin, editors), Leningrad, USSR, pp. 173–180, October 17–21, 1989, Dordrecht, The Netherlands: Kluwer, 1990.

[24] X X Newhall, R. A. Preston, and P. B. Esposito, "Relating the JPL VLBI Reference Frame and the Planetary Ephemerides," *Astrometric Techniques,* proceedings of the 109th IAU Symposium (H. K. Eichhorn and R. J. Leacock, editors), Gainesville, Florida, pp. 789–794, January 9–12, 1984, Dordrecht, The Netherlands: D. Reidel, 1986.

[25] W. M. Folkner et al., "Determination of the Extragalactic-Planetary Frame Tie from Joint Analysis of Radio Interferometric and Lunar Laser Ranging Measurements," *Astronomy and Astrophysics,* vol. 287, no. 1, pp. 279–289, July 1994.

[26] J. S. Border, "Venus Ephemeris Measurements and Frame-Tie using Magellan ΔDOR," JPL Interoffice Memorandum 335.1-94-032 (internal document), Jet Propulsion Laboratory, Pasadena, California, September 6, 1994.

[27] J. S. Border and J. A. Koukos, "Technical Characteristics and Accuracy Capabilities of Delta Differential One-Way Ranging (ΔDOR) as a Spacecraft Navigation Tool," CCSDS B20.0-Y-1, *Report of the Proceedings of the RF and Modulation Subpanel 1E Meeting at the German Space Operations Centre: September 20–24, 1993* (T. M. Nguyen, editor), Yellow Book, Oberpfaffenhofen, Germany: Consultative Committee for Space Data Systems, February 1994.

[28] N. F. deGroot, "Radio Frequency Selection and Radio Interference Prevention," chapter in *Deep Space Telecommunications System Engineering* (J. H. Yuen, editor), New York: Plenum Press, 1983.

[29] J. S. Border et al., "Determining Spacecraft Angular Position with Delta VLBI: The Voyager Demonstration," AIAA-82-1471, paper presented at the AIAA/AAS Astrodynamics Conference, San Diego, California, August 9–11, 1982.

[30] E. J. Graat, M. S. Ryne, J. S. Border, and D. B. Engelhardt, "Contribution of Doppler and Interferometric Tracking During the Magellan Approach to Venus," AAS 91-394, *Advances in the Astronautical Sciences, Volume 76, Part II* (B. Kaufman, K. T. Alfriend, R. L. Roehrich, and R. R. Dasenbrock, editors), proceedings of the AAS/AIAA Astrodynamics Specialist Conference, Durango, Colorado, pp. 919–940, August 19–22, 1991.

[31] Mars Climate Orbiter Investigation Board, *Report on Project Management in NASA,* March 13, 2000, p. 17, http://www.ksc.nasa.gov/mars/msp98/misc/MCO_MIB_Report.pdf Accessed September 13, 2000.

[32] W. M. Folkner et al., "Earth-Based Radio Tracking of the Galileo Probe for Jupiter Wind Estimation," *Science,* vol. 275, no. 5300, pp. 644–646, January 31, 1997.

[33] J. S. Border, "Data Acquisition for the Mars Polar Lander DDR Experiment," JPL Interoffice Memorandum 335.1-99-015 (internal document), Jet Propulsion Laboratory, Pasadena, California, December 27, 1999.

[34] L. A. Cangahuala et al., "Mars Polar Lander Operations: Navigation Advisory Group Activities," MS00/P21, *Proceedings of the Inter-*

national Symposium on Space Dynamics, CNES, Biarritz, France, June 26–30, 2000.

[35] S. T. Lowe and J. S Border, "Analysis of Stanford's Jan-4 MPL Signal Candidate," JPL Interoffice Memorandum 335.4-2000-001 (internal document), Jet Propulsion Laboratory, Pasadena, California, March 2, 2000.

Chapter 5
Future Directions in Radiometric Tracking

5.1 Doppler and Range

The precision, versatility, and availability of Doppler measurements have made them the primary tracking data type in the past and will ensure an important future role as well. The advent of X-band uplinks and X-band spacecraft transponders has improved the precision of Doppler observables by a factor of 13 relative to S-band links, due to the reduced effect of charged particles at the higher frequency. If Ka-band radio links are employed, charged-particle effects will decrease, and Doppler measurement precision will improve further. These improvements in accuracy make it possible to better characterize small forces that act on spacecraft, such as those arising from solar pressure, attitude maneuvers, momentum wheel desaturation maneuvers, or gas leaks. However, improvement of dynamic force models in three dimensions may not be possible because of the limited geometry associated with Earth-based Doppler tracking; therefore, improved Doppler data accuracy alone does not guarantee improved radio navigation.

Two-way tracking, where the same ground-based frequency standard is used as the reference for both the uplink signal and for the downlink detector, provides the best Doppler data accuracy today. However, improvements in the stability of flight oscillators may eventually make one-way Doppler tracking competitive with two-way tracking [1]. (This improvement might be achieved through the development of passive linear ion-trap resonators [2] although at the time of publication, flight experiments with these devices are at least 5 years in the future.[1]) One-way tracking simplifies ground-based operations

[1] R. L. Tjoelker, personal communication, Tracking Systems and Applications Section, Jet Propulsion Laboratory, Pasadena, California, May 2000.

and offers a better SNR for the reception of spacecraft telemetry data. The improvement to the telemetry SNR is due to two factors. First, one-way transmissions provide better short-term (< 1 s) stability, resulting in less signal loss in the detection process. This is because the short-term stability of two-way transmissions is degraded by solar plasma scintillations of the uplink signal and, for more distant spacecraft, by thermal noise in the spacecraft receiver. Second, the ground antennas are configured in a listen-only mode for one-way tracking, whereas the more complicated diplexer mode, required for simultaneous uplinking and downlinking, increases the effective system noise temperature of the ground receiver.

One-way tracking has another advantage, with far-reaching consequences. For future missions in which several spacecraft are in orbit about or landed on the same planet, a single deep space antenna can acquire one-way Doppler and telemetry simultaneously from all spacecraft. Multiple uplink signals are not required. Consequently, this configuration results in more efficient use of ground-based resources and enhances orbit solutions and lander position estimates through the use of differential measurements. Simultaneous observations of multiple spacecraft are discussed further in Section 5.4.

Range measurement accuracy is limited today by uncalibrated delays in analog components of spacecraft transponders and ground receivers. Calibration accuracy of the station delay has improved over the last decade, from about 5 m to about 2 m. While precision would appear to be better than 2 m, errors at the 2-m level were still apparent in the mid-to-late 1990s in the Ulysses dual-frequency range data[2] and in Pathfinder X-band data from the Mars surface [3]. Further reduction of this systematic error component may remain a challenge due to the narrow bandwidth of deep space ranging codes. At the same time, an improvement in link margin and a reduction in the random measurement error are expected as future transponders provide a regenerative ranging capability [4]. Nonetheless, systematic errors at the meter level, due primarily to uncalibrated instrumental effects, are likely to remain.

Combining range and interferometric observables is an alternative to using long, continuous Doppler arcs for cruise navigation. In this method, the three components of spacecraft position are directly measured in just a few minutes, using range and interferometry. Doppler data may then be applied to infer better force models, without the fear of aliasing model parameters into weakly observed spacecraft state components. In addition, simultaneously fitting all data types leads to improved navigation reliability and robustness. Furthermore, if they were available, range measurements with submeter accuracy would have application to the relative tracking of planetary orbiters, rovers and landers [5].

---

[2]W. M. Folkner, personal communication, Tracking Systems and Applications Section, Jet Propulsion Laboratory, Pasadena, California, April 2000.

5.2 Very Long Baseline Interferometry

The first-generation operational DSN VLBI system has provided angular spacecraft measurements with an accuracy of better than 50 nrad. The next-generation system implementation incorporates numerous design improvements to increase the operability, reliability, and accuracy of VLBI measurements. Utilizing spacecraft DOR tones with a spanned bandwidth of 38 MHz, VLBI observable precision and instrumental calibration will be at the 5 nrad level or better. Measurements of ΔDOR at this accuracy level are expected to contribute to the approach navigation for orbiters and landers being delivered to Mars and elsewhere.

The VSR (the next-generation VLBI system) is based on the Full Spectrum Recorder. The FSR is an open-loop receiver that can downconvert and record selected portions of the RF spectrum. The FSR has been used in the DSN for Galileo telemetry arraying since 1996 [6,7] and has an outstanding record in terms of reliability and operability. Real-time spectrum displays are used to verify signal acquisition. In addition, internal timing and precision are designed to allow combining of signals from multiple antennas spanning intercontinental distances. The algorithms used in arraying to align the signals prior to combining are closely related to those used for VLBI signal processing; therefore it is a small conceptual step to evolve the FSR into a VLBI system.

The FSR has open-loop multiple-channel recording capability. The input is a broadband intermediate-frequency signal that has been downconverted from radio frequency. This input is digitally sampled at 256 Msamples/s. All subsequent downconversion and filtering steps are digital. This preserves the phase relationship between components of the signal being measured (for example, DOR tones) and eliminates the introduction of instrumental errors during baseband downconversion and filtering. Up to four independent channels of bandwidth, 16 MHz each, may be placed anywhere within the 128-MHz input. Selected portions of the baseband channels may be recorded in bandwidths ranging from 1 kHz up to 16 MHz. From 1 to 16 bits/sample may be selected. Typical operation is expected to record four channels of spacecraft data, centered on the carrier and DOR tones, at 8 bits/sample and 2 Ksamples/s. Quasar data would be recorded in four channels centered at the same frequencies, using 2 bits/sample and 2 Msamples/s. This recording strategy is chosen to balance errors caused by dispersive instrumental effects against errors caused by SNR.

The higher channel sampling rate, multibit samples, and the use of parallel rather than time-multiplexed channels are the keys to improved measurement precision. In the example cited in Fig. 4-2, the error due to quasar SNR was 9 nrad, using the NCB VLBI system and assuming a source strength of 0.4 Jy, a 70-m and 34-m DSN antenna pair, and 10-min integration time. With the VSR,

that error drops to 3 nrad, still assuming a source strength of 0.4 Jy, but now using a 34-m and 34-m DSN antenna pair and 20-min integration time.

Recorded data are transmitted through the Ground Communication Facility to the Network Operations Control Center at JPL, where data from two stations are combined to form interferometric measurements. At data transmission rates readily achieved today, future observables could be delivered to navigation teams within an hour of data acquisition.

Angular measurements accurate to better than 50 nrad will continue to require quasar observations. Even though interstation clock synchronization approaches the nanosecond level today using GPS, path delays through the specific instrumentation used to record spacecraft tracking data cannot be known a priori to this level. A real-time calibration is required. For intercontinental VLBI measurements, quasar signals are the reliable and available source for instrumental calibration.

The VLBI system upgrade, scheduled for 2001, and the calibration system improvements discussed in Section 3.4 both contribute to improved ΔDOR accuracy. Figure 4-2 contrasts the performance of the previous VLBI system, using calibrations available in 1992, and the next VLBI system, labeled 2001, using calibrations available today. The figure shows an example of performance corresponding to the assumptions given in Tables 3-3 and 4-1. Actual performance, however, may vary by a factor of two or more, depending on specific geometry and spacecraft hardware.

5.3 Connected-Element Interferometry

Interferometry using antennas separated by tens to hundreds of kilometers has the potential to determine spacecraft angular position at the 50-nrad level [8]. When all system elements are connected via high-speed data lines to a local real-time correlator, the technique is known as connected-element interferometry (CEI). When CEI is used, it is possible to obtain observables in real time at the tracking site. Moreover, on-site processing allows real-time validation of successful data acquisition, a feature highly desired by DSN operations personnel and the flight projects.

CEI performance depends heavily upon the separation of the receiving antennas. At present, separations between operational stations within any of the three DSN complexes are less than 10 km; hence, the DSN is currently unable to support this type of measurement. There is, however, at the Goldstone complex, a telecommunications research and development station that is 21 km from the other antennas. Tests conducted at Goldstone demonstrate the utility of CEI for navigation [9]. An array of antennas spread out over a suitable distance could provide this capability.

5.4 Same-Beam Interferometry

When two spacecraft are so close in an angular sense that they may be observed in the same beamwidth of an Earth-based radio antenna, differential interferometric observables may be generated using simultaneous observations of the two spacecraft from two deep space antennas. This technique, illustrated in Fig. 5-1 and known as same-beam interferometry (SBI), provides extremely accurate relative position measurements in the plane-of-the-sky, complementing the line-of-sight information from Earth-based Doppler and range measurements. System errors that scale with angular and temporal separations are greatly reduced, allowing nearly the full precision of carrier-phase measurements to be utilized. The concept of differential tracking for angularly close sources is well established and has been applied to numerous astronomical problems [10–13]. Furthermore, improved orbit determination using this technique was demonstrated with the Pioneer Venus and Magellan orbiters at Venus [14,15]. The next-generation VLBI system implementation, described in Section 5.2, could provide the means for operational use of this technique.

As more spacecraft begin operating at Mars, SBI could be used to improve orbit determination while requiring fewer Earth-based tracking resources. All spacecraft within Mars stationary orbit would be visible within the 1-mrad beamwidth of a 34-m antenna at X-band. All signals would be acquired simultaneously. SBI data acquired during ground-station overlaps could provide enough geometric data strength to offset the loss of long arcs of ground-based two-way Doppler measurements. One-way Doppler combined with SBI may meet navigation requirements, eliminating the need for multiple uplinks.

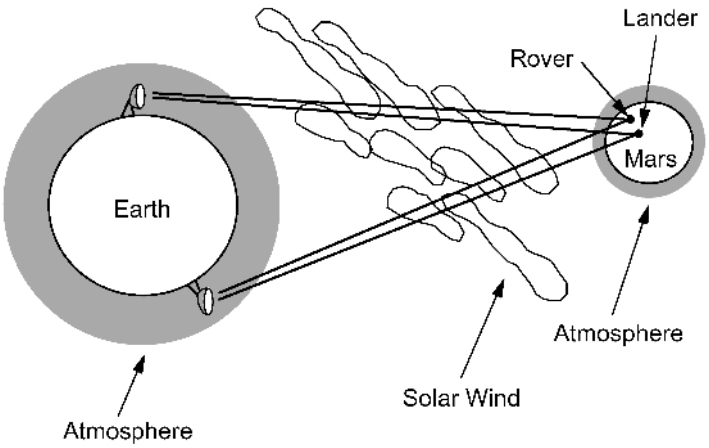

Fig. 5-1. Same-beam interferometry measurement geometry.

SBI offers a significant performance advantage over conventional spacecraft-to-quasar ΔDOR. Figure 5-2 shows an error budget for SBI measurements of two Mars orbiters. Some appreciation of the accuracy improvements afforded by this technique can be gained by contrasting Figs. 4-2 and 5-2. In Fig. 5-2, the dominant SBI error is due to solar plasma; this error does not cancel as completely as other media errors, since the four SBI ray paths are at a maximal spatial separation in the interplanetary space between Earth and Mars. A 20-deg Sun-Earth-probe angle and 5-min data averaging were assumed for this calculation. For an Earth-Mars distance of 1.5 astronomical units (AUs), the root-sum-square (rss) error of 36 prad corresponds to an 8-m error in the determination of one component of the relative position of the two spacecraft.

Also shown in Fig. 5-2 is an error budget for two vehicles on the surface of Mars. The SBI measurement accuracy for a rover and lander is a factor of three better than that for two orbiters. The difference is due to the much smaller angular separation between the rover and the lander. Differential data from a landed spacecraft and from an orbiter help to determine the absolute position of a spacecraft on the surface of Mars, especially the distance from the equatorial

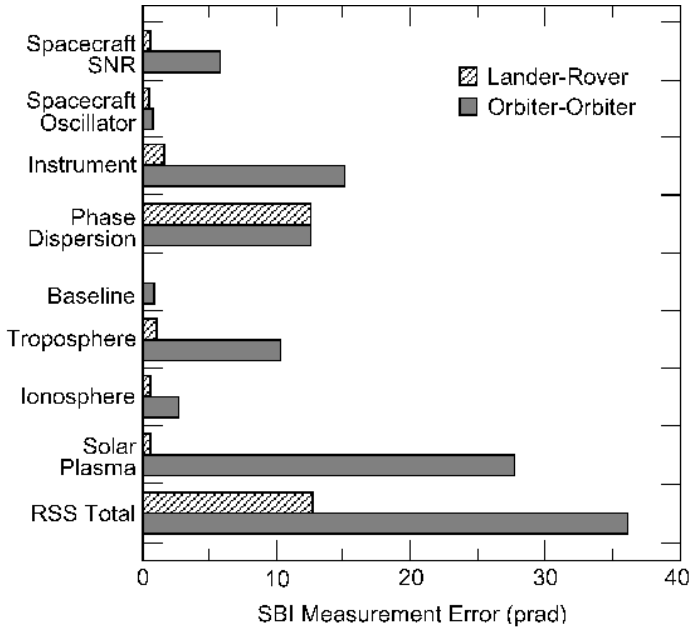

Fig. 5-2. Error budget for same-beam interferometry measurements for a lander and rover on the surface of Mars and for two spacecraft in orbit about Mars. X-band radio links and a Sun-Earth-probe angle of 20 deg are assumed.

plane. Using SBI, the position of the landed spacecraft is established with respect to the center of mass of Mars because differential data tie it to the orbiter, which is itself tied to the Mars center of mass through dynamics.

Although in situ measurements may become the primary technique for precise positioning of vehicles on the surface, SBI could be useful as part of a global navigation strategy or as a backup capability.

5.5 Spacecraft-to-Spacecraft Tracking

Historically, interspacecraft metric tracking has seen only limited use in the planetary exploration program. However, the recent emergence of mission concepts involving constellations of spacecraft flying in precise formation (such as the planned interferometry missions of the NASA Origins Program) and the expected need for highly accurate close proximity and/or in situ tracking in Earth orbit, at Mars, and elsewhere, have prompted the design of new flight instruments for interspacecraft microwave tracking and communications. Receivers and transceivers for the most demanding microwave tracking applications will benefit from two decades of GPS precise tracking technologies.

Beginning in the early 1980s, JPL developed the Rogue family of GPS ground receivers. These receivers were initially built to provide ionospheric calibrations at the DSN tracking complexes. The Rogue design also met the needs of the geodetic community for precise measurement of crustal motion and precise positioning of low Earth orbiters. Ground-breaking performance was achieved through the use of new digital technology that allowed simultaneous, dual-frequency tracking of both carrier phase and pseudorange from as many as eight GPS satellites. The receivers used P-code when it was available, but could switch to codeless operation when the military turned on antispoofing [16].

The TurboRogue family of receivers was an extension of the Rogue design; it was developed primarily by the NASA Solid Earth and Natural Hazards Program. These receivers incorporated emerging compact, low-power, digital technology to substantially reduce receiver size, weight, and power [17]. These characteristics enabled portable operations and access to remote areas. Performance enhancements also made the TurboRogue attractive for fixed ground network operations, and many have been installed in the IGS global network [18]. Modified versions of the TurboRogue were flown on several satellites, beginning with the GPS Meteorology Experiment, known as GPSMET [19].

More recently, a family of flight receivers has been developed at JPL as an extension of the TurboRogue family of GPS ground and flight receivers [20]. The new receivers, generically referred to as the Blackjack family, are designed to support precision orbit determination for altimetric, radar, and other remote-sensing missions, and to also provide valuable measurements of Earth's atmo-

sphere and ionosphere [21–23]. Using as many as 16 parallel channels, they simultaneously acquire dual-frequency GPS carrier-phase and pseudorange measurements. These measurements have improved precision relative to the TurboRogue measurements, due to the addition of a patented, enhanced-codeless tracking technique [24].

For NASA's 2001 Gravity Recovery and Climate Experiment (GRACE) mission, the receive-only GPS instrument design described above has been altered to include satellite cross-link ranging capability and star tracker processing [25]. GRACE will place two satellites separated by about 220 km in coplanar, near-polar orbits, at an altitude of 300 to 500 km. Precise measurements of the differential gravitational effects on the spacecraft, detected through variations in their separation, will enable determination of the Earth's gravity field to unsurpassed accuracy and resolution [26]. The GPS tracking data acquired on each satellite will enable precise orbit determination, while the intersatellite ranging and two accelerometers (one on each spacecraft) will provide the required gravity field information. GRACE mission requirements mandate that spacecraft separation need only be controlled to $\pm$ 50 km, but variations in separation must be measured to a precision of a few microns [26]. The cross-link radio design provides transmit and receive capability at 24.5 GHz and 32.7 GHz, enabling biased range measurements with approximately one-micron precision [27].

The interspacecraft tracking concept is central to the design of a related instrument, referred to as the Autonomous Formation Flyer (AFF). The first AFF, termed the Constellation Communications and Navigation Transceiver (CCNT), will fly on Space Technology 5 (ST-5), a NASA 2003 mission to demonstrate nanosatellite constellation technologies. This mission will fly three satellites in highly elliptical Earth orbits having 200-km perigee and ~ 40,000-km apogee, with the objective of measuring the effects of the Sun on Earth's magnetic field. The CCNT will provide communication as well as cross-link ranging.

Another version of the AFF will fly on ST-3, to be launched in 2005. This mission will place two spacecraft in formation at the libration point, L1, of the Sun-Earth system. The primary objective of the mission is to validate technologies leading to a future deep space constellation in tight formation, called Terrestrial Planet Finder [28]. The AFF, with a Ka-band cross-link and three antennas on each spacecraft, will provide coarse relative positioning of the two spacecraft to an accuracy of 1 cm and bearing information to an accuracy of 1 arcmin. A separate optical metrology unit with a precision of 1 nm will then enable spacecraft control to 5 cm [29].

A transceiver derived from the AFF and designed for cross-link communication and precise range and range rate capability has been under study for a future communications and tracking network at Mars. The envisioned "Mars-

net" would feature as many as six satellites in low orbit (~800 km) and possibly another in areostationary orbit. This network could communicate with science orbiters, incoming spacecraft, or landers and rovers on the surface of Mars that carry compatible radio systems [30]. While the network transceivers could be capable of autonomous, onboard orbit determination and operation, initial satellite operations would most likely be supported autonomously on Earth. Marsnet users, equipped with compatible radios, could receive range and range rate data, as well as satellite ephemeris information, from all orbiters in view.

From a navigation perspective, the potential benefits of such a constellation are impressive. Spacecraft approaching Mars could use onboard ranging to one or more orbiters for real-time determination of position prior to aerocapture or entry-descent-landing exercises. Early study results indicate that the use of one-way Doppler data from a single Mars orbiter could enable radio-only position determination one day prior to encounter to 200–300 m,[3] which is an improvement of nearly an order of magnitude, relative to Earth-based tracking strategies. These results assume that both spacecraft carry an ultrastable state-of-the-art oscillator. Entry-descent-landing capability using the Marsnet would depend upon constellation design, particularly the number of satellites in common view of the user. For example, with continuous tracking from three properly spaced Marsnet orbiters at 800 km, a descending spacecraft equipped with a network transceiver and an inertial measurement unit (IMU) could determine its position in near-real time (1-min latency) to 50 cm or better.[4] With only two-satellite coverage, this accuracy degrades to the meter level. Likewise, elements on the surface with three or more Marsnet satellites in view, could determine their positions in near-real time to a few decimeters.[5]

The transceiver concept envisioned for the Marsnet has broad implications for future space missions. First, integrated tracking and communications functionality will ensure the concept's multimission utility while conserving spacecraft power and mass. Second, high-precision radiometric tracking capability, including range, range rate, and direction-finding measurements, will be attractive for complex navigation applications involving multiple spacecraft. Third, the architecture inherited from the GPS Blackjack receiver is highly adaptable and configurable. This flexibility can be attributed to its software-intensive modular design, which enables additional capabilities to be readily incorporated, even during flight. For a relatively long-lifetime instrument, the ability to upgrade in flight can be quite valuable. Moreover, the ease with which new

---

[3] T. A. Ely, personal communication, Navigation and Flight Mechanics Section, Jet Propulsion Laboratory, Pasadena, California, July 2000.

[4] Y. E. Bar-Sever, personal communication, Tracking Systems and Applications Section, Jet Propulsion Laboratory, Pasadena, California, July 2000.

[5] Ibid.

requirements can be added to the existing architecture will translate into cost savings for future missions. As an example, the upcoming Laser Interferometer Space Antenna (LISA) mission (scheduled to launch in 2009) [31] will require metrology precision to the level of picometers and control to the level of nanometers. To accomplish this, the transceiver can be adapted to utilize an optical ranging system together with the existing baseband processor.

In summary, future deep space missions are expected to place new requirements on flight communications and navigation systems. The highly precise formation control of space interferometers as well as stringent navigation requirements at Mars and other target bodies will continue to drive the development of more capable flight transceivers. Consequently, spacecraft-to-spacecraft tracking and communications technologies are likely to receive unprecedented emphasis during the first decade of the 21st century.

References

[1] J. S. Border and E. R. Kursinski, "Deep Space Tracking and Frequency Standards," *Proceedings of the IEEE 45th Annual Symposium on Frequency Control,* IEEE 91CH2965-2, Los Angeles, California, pp. 594–607, May 29–31, 1991.

[2] R. L. Tjoelker, J. D. Prestage, and L. Maleki, "Improved Timekeeping using Advanced Trapped Ion Clocks," *Proceedings of the 31st Conference on Precise Time and Time Interval (PTTI),* Dana Point, California, pp. 597–604, December 7–9, 1999.

[3] W. M. Folkner, C. F. Yoder, D. N. Yuan, E. M. Standish, and R. A. Preston, "Interior Structure and Seasonal Mass Redistribution of Mars From Radio Tracking of Mars Pathfinder," *Science,* vol. 278, no. 5344, pp. 1749–1752, December 5, 1997.

[4] J. B. Berner et al., "Regenerative Pseudo-Noise Ranging for Deep Space Applications," *TMO Progress Report 42-137,* vol. January–March 1999, http://tmo.jpl.nasa.gov/progress_report/issues.html Accessed October 16, 2000.

[5] R. D. Kahn, W. M. Folkner, C. D. Edwards, and A. Vijayaraghavan, "Position Determination of a Lander and Rover at Mars With Earth-Based Differential Tracking," *TDA Progress Report 42-108,* vol. October–December 1991, http://tmo.jpl.nasa.gov/progress_report/issues.html Accessed October 16, 2000.

[6] T. T. Pham et al., "Tracking the Galileo Spacecraft With the DSCC Galileo Telemetry Prototype," *TDA Progress Report 42-119,* vol. July–September 1994, http://tmo.jpl.nasa.gov/progress_report/issues.html Accessed October 16, 2000.

[7] T. T. Pham, A. P. Jongeling, and D. H. Rogstad, "Enhancing Telemetry and Navigation Performance with Full Spectrum Arraying," *2000 IEEE Aerospace Conference Proceedings,* Big Sky, Montana, pp. 491–498, March 18–25, 2000.

[8] C. D. Edwards, "Angular Navigation on Short Baselines Using Phase Delay Interferometry," *IEEE Transactions on Instrumentation and Measurement,* vol. 38, no. 2, pp. 665–667, April 1989.

[9] C. D. Edwards et al., "The Goldstone Real-Time Connected Element Interferometer," *TDA Progress Report 42-110,* vol. April–June 1992, http://tmo.jpl.nasa.gov/progress_report/issues.html Accessed October 16, 2000.

[10] C. C. Counselman, III, H. F. Hinteregger, and I. I. Shapiro, "Astronomical Applications of Differential Interferometry," *Science,* vol. 178, no. 4061, pp. 607–608, November 10, 1972.

[11] R. W. King, C. C. Counselman, III, and I. I. Shapiro, "Lunar Dynamics and Selenodesy: Results from Analysis of VLBI and Laser Data," *Journal of Geophysical Research,* vol. 81, no. 35, pp. 6251–6256, December 10, 1976.

[12] J. R. Smith and R. Ramos, "Data Acquisition for Measuring the Wind on Venus from Pioneer Venus," *IEEE Transactions on Geoscience and Remote Sensing,* vol. GE-18, no. 1, pp. 126–130, January 1980.

[13] R. A. Preston et al., "Determination of Venus Winds by Ground-Based Radio Tracking of the VEGA Balloons," *Science,* vol. 231, no. 4744, pp. 1414–1416, March 21, 1986.

[14] J. S. Border, W. M. Folkner, R. D. Kahn, and K. S. Zukor, "Precise Tracking of the Magellan and Pioneer Venus Orbiters by Same-Beam Interferometry, Part I: Data Accuracy Analysis," *TDA Progress Report 42-110,* vol. April–June 1992, http://tmo.jpl.nasa.gov/progress_report/issues.html Accessed October 16, 2000.

[15] W. M. Folkner, J. S. Border, S. Nandi, and K. S. Zukor, "Precise Tracking of the Magellan and Pioneer Venus Orbiters by Same-Beam Interferometry—Part II: Orbit Determination Analysis," *TDA Progress Report*

42-113, vol. January–March 1993, http://tmo.jpl.nasa.gov/progress_report/issues.html Accessed October 16, 2000.

[16] T. K. Meehan et al., "ROGUE: A New High Accuracy Digital GPS Receiver," paper presented at the IUGG XIXth General Assembly, Vancouver, British Columbia, August 9–22, 1987.

[17] T. K. Meehan et al., "The TurboRogue Receiver," *Sixth International Geodetic Symposium on Satellite Positioning,* Columbus, Ohio, pp. 209–218, March 17–20, 1992.

[18] International GPS Service, http://igscb.jpl.nasa.gov/igscb/station/general/rcvr_ant.tab Accessed September 12, 2000.

[19] R. Ware et al., "GPS Sounding of the Atmosphere from Low Earth Orbit: Preliminary Results," *Bulletin of American Meteorological Society,* vol. 77, no. 1, pp. 19–40, January 1996.

[20] T. K. Meehan et al., "GPS on a Chip—An Advanced GPS Receiver for Spacecraft," *ION-98,* Nashville, Tennessee: Institute of Navigation, September 1998.

[21] W. I. Bertiger et al., "Precise Orbit Determination for the Shuttle Radar Topography Mission using a New Generation of GPS Receiver," *Proceedings of ION GPS-2000,* Salt Lake City, Utah, September 19–22, 2000, in press.

[22] D. J. Chelton, J. Ries, B. J. Haines, L.-L. Fu and P. S. Callahan, "Satellite Altimetry," chapter in *Satellite Altimetry and Earth Sciences* (L.-L. Fu and A. Cazenave, editors), San Diego, California: Academic Press, October 2000.

[23] W. G. Melbourne et al., *The Application of Spaceborne GPS to Atmospheric Limb Sounding and Global Change Monitoring,* JPL Publication 94-18, Jet Propulsion Laboratory, Pasadena, California, April 1994.

[24] T. K. Meehan et al., "P-code Enhanced Method for Processing Encrypted GPS Signals Without Knowledge of the Encryption Code," U.S. Patent 6061390, May 9, 2000.

[25] E. S. Davis et al., "The GRACE Mission: Technical Challenges," IAF-99-B.2.05, paper presented at the 50th International Astronautical Congress, Amsterdam, The Netherlands, October 4–8, 1999.

[26] *GRACE Science and Mission Design Document,* JPL D-15928, Rev. B (internal document), Jet Propulsion Laboratory, Pasadena, California, April 15, 1999.

[27] J. B. Thomas, *An Analysis of Gravity-Field Estimation Based on Intersatellite Dual-1-Way Biased Ranging,* JPL Publication 98-15, Jet Propulsion Laboratory, Pasadena, California, May 1999.

[28] *The Terrestrial Planet Finder (TPF): A NASA Origins Program to Search for Habitable Planets* (C. A. Beichman, N. J. Woolf, and C. A. Lindensmith, editors), JPL Publication 99-3, Jet Propulsion Laboratory, Pasadena, California, May 1999.

[29] G. H. Blackwood, S. Dubovitsky, R. P. Linfield, and P. W. Gorham, "Interferometer Instrument Design for New Millennium Deep Space 3," Paper no. 3350-83, *Astronomical Interferometry,* proceedings of the SPIE, vol. 3350, Kona, Hawaii, pp. 173–183, March 20–24, 1998.

[30] T. A. Ely et al., "Mars Network Constellation Design Drivers and Strategies," AAS 99-301, *Advances in the Astronautical Sciences, Volume 103, Part I* (K. C. Howell, F. R. Hoots, B. Kaufman, K. T. Alfriend, editors), proceedings of the AAS/AIAA Astrodynamics Specialist Conference, Girdwood, Alaska, pp. 17–32, August 16–19, 1999, San Diego, California: Univelt, 1999.

[31] *Laser Interferometer Space Antenna (LISA) Pre-Phase A Report,* 2nd edition, MSQ 233, Garching, Germany: Max-Planck-Institute for Quantum Optics, July 1998.

Glossary

barycenter	The center of mass of a system of particles or bodies.
coherent	Pertaining to two radio signals in a relationship such that one is an exact numeric multiple of the other.
declination	In astronomical spherical coordinates, the angle above or below the plane passing through the origin of the coordinate system and normal to the polar axis.
ecliptic	The plane containing the orbit of Earth about the Sun.
ephemeris	A representation of the position, within a defined reference system, of a planet, moon, or spacecraft as a function of time.
epoch	An instant in time that defines an event.
fiducial station	A tracking station whose location is held fixed for the purposes of data processing.
maser	A microwave device that, when stimulated by a weak signal, will emit a stronger signal at a related frequency. Derived from *m*icrowave *a*mplification by *s*timulated *e*mission of *r*adiation.
mean equator and equinox	Reference frame models that account for only precession.
nutation	The short-period (a few decades or less) motion of Earth's spin axis, expressed in inertial coordinates.
observable	A quantity, such as time or distance, determined from a measurement.
phase-locked loop	An algorithm to adjust a local reference signal so that it maintains a constant phase relationship with an input signal.
plane-of-the-sky	A plane containing the spacecraft that is orthogonal to the line of sight from the observer to the spacecraft.
precession	The long-period (centuries) motion of Earth's spin axis, expressed in inertial coordinates.

quasar A quasistellar extragallactic object that emits powerful radio waves.

residual The difference between an observed and a modeled value.

right ascension In astronomical coordinates, the angle about the polar axis, measured from a defined origin.

topocentric Pertaining to a measurement from the surface of a reference body.

true equator and equinox Reference frame models that account for both precession and nutation.

Acronyms

AAM	atmospheric angular momentum
AAS	American Astronomical Society
AFF	Autonomous Formation Flyer
AIAA	American Institute of Aeronautics and Astronautics
AU	astronomical unit
CA	clear acquisition
CCNT	Constellation Communications and Navigation Transceiver
CEI	connected-element interferometry
CIO	Conventional International Origin
CSO	compensated sapphire oscillator
DoD	Department of Defense
DOR	differential one-way range
DRVID	differenced range versus integrated Doppler
DSN	Deep Space Network
FSR	Full Spectrum Recorder
FTS	Fourier Transform Spectrometry
GGN	Global GPS Network
GIM	global ionosphere mapping
GPS	Global Positioning System
GPSMET	GPS Meteorology Experiment
GRACE	Gravity Recovery and Climate Experiment
IAA	International Academy of Astronautics
IAF	International Astronautical Federation
IAIN	International Aerospace Information Network
IAU	International Astronomical Union
ICRF	International Celestial Reference Frame
IEEE	Institute of Electrical and Electronics Engineers
IERS	International Earth Rotation Service
IGS	International GPS Service
IMU	inertial measurement unit
IOM	interoffice memorandum

ION	Institute of Navigation
ITRF	International Terrestrial Reference Frame
IUGG	International Union of Geodesy and Geophysics
Jy	Jansky; a measure of flux density
KEOF	Kalman Earth Orientation Filter
LISA	Laser Interferometer Space Antenna
LITS	linear ion-trap standard
LLR	lunar laser ranging
LOD	length of day
MPL	Mars Polar Lander
NCB	Narrow Channel Bandwidth
PM	polar motion
PMX	x-component of polar motion
PMY	y-component of polar motion
RF	radio frequency
rms	root-mean-square
rss	root-sum-square
RTLT	round-trip light time
RU	range unit
SA	selective availability
SBI	same-beam interferometry
SLR	satellite laser ranging
SNR	signal-to-noise ratio
TDA	Telecommunications and Data Acquisition
TEC	total electron count
TECU	total electron count unit
TMO	Telecommunications and Mission Operations
URSI	International Union of Radio Science
UT	correction to universal time: UT1−UTC
UT1	universal time one
UTC	universal time coordinated
VLBI	very long baseline interferometry
VSR	VLBI Science Receiver
WVR	water vapor radiometer

JPL Publication 00-11